SPWLA-France workshop on Acoustics
March 31st at SGF_PARIS

DSI Anisotropy: Historical DSI case studies
by Charles Naville, IFPEN; 14h30-15h ;

Part 1- Introduction

Initial dipole sonic data processing results were obtained in 1993
by **JP Yver & D. Belaud, SCHLUMBERGER- France,**

Implementing an S-wave birefringence Anisotropy detection method of azimuthal STC slowness Rotation-Scan computed over the array of receivers,
using a 15° azimuthal step over a 180° azimuthal range
with SCR acquired data = 4 levels of (X,Y) sensors recorded simultaneously, for each EX, then EY source activations (2 records)

In parallel, in the early 1990's, C. Esmersoy, M. Kane & al., SCHLUMBERGER-USA were entrusted with developing an S-wave dection method, based on *minimisation of the cross-dipole energy for the flexural S-wave propagation between dipole sources and the receiver array,*
with BCR acquired data = 8X, then 8Y sensors recorded simultaneously for each EX, then EY source activations (4 records)

The results from the two methods show notable differences, better understood at present time, however differences remain due to the different detection principles
and different S-wave propagation assumptions…
even with modern array sonic tools recording in STC mode with an array of 13 receiver levels and higher dynamic range (20 bit or 24 bit/ sample , versus 12 bit/sample for the initial DSI tool)

S-wave BIREFRINGENCE or Shear-wave SPLITTING

The Ordinary BIREFRINGENCE concerns the propagation of two linear orthogonal eigen S-wave modes, (not elliptical) characterized by the following parameters:

1. Direction of Fast Split S-wave (Not always correct)
2. Time lag between the two eigen S-wave modes or Velocity anisotropy: $\Delta V/V = 2(V2-V1/V1+V2)$, in %
3. Differential attenuation, or Attenuation anisotropy, *between principal split S-wave modes, at same frequency, linear scale or Decibel* . Parameter still not computed

These three attributes can generally be computed :

- either from dipole sonic, 3-Component (3C) - VSP,
- or from 3C-reflection surface seismic,
- or from microseisms and Earthquakes.

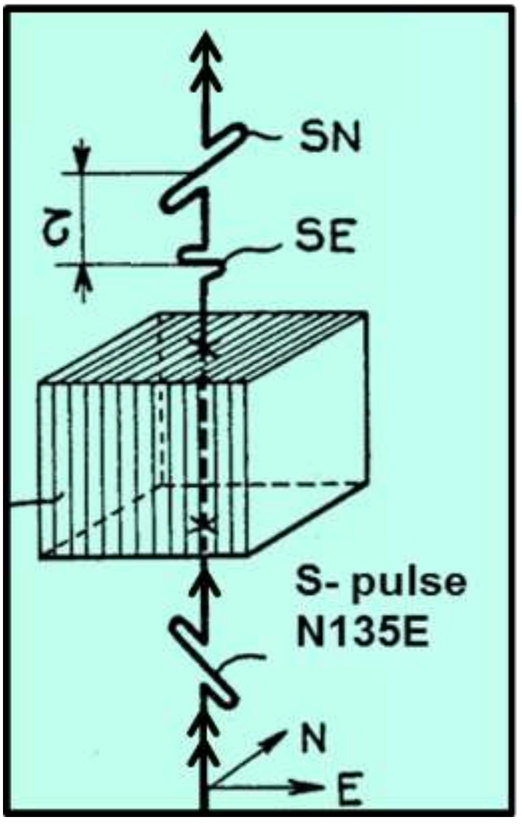

The vertically laminated medium on the left presents an azimuthal anisotropy. The incident S-wave linear pulse polarized N135°E splits into an S-N fast S-wave polarized parallell to the streaks , and a W-E slower S-wave polarized orthogonally, delayed by a time lag τ, and more attenuated than S-fast

Figure from Naville C. (1986), and Pat. US 4,789,969 (1988).

DSI: Dipole Shear Sonic Imager Tool

Fig I-2

The dipole section of this tool consists of an array of eight dipole receiver levels, and two orthogonal dipole sources

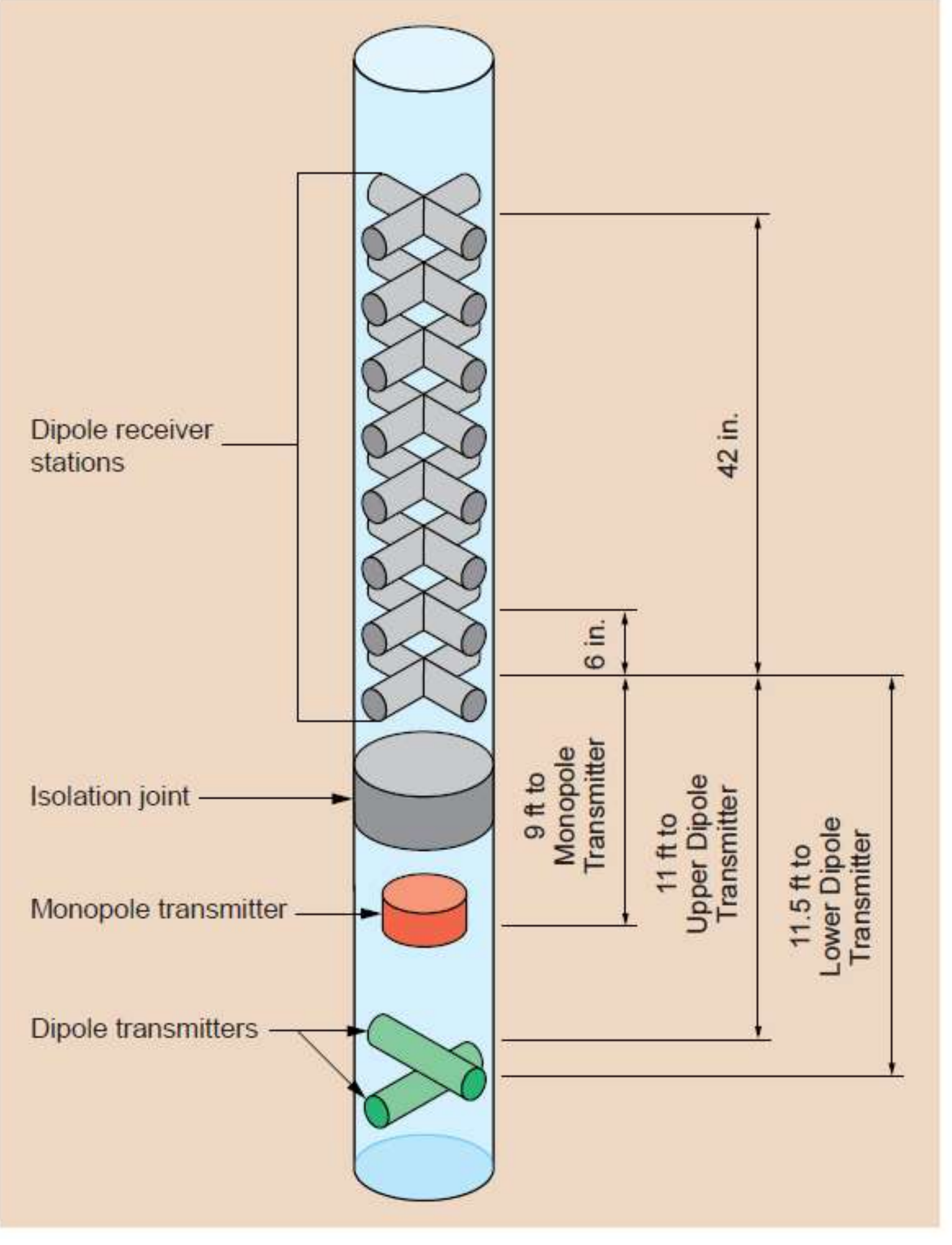

Figure from D. Belaud and E. Standen (1995)

Dipole Array Sonic tool in the borehole

Fig I-3

TWO birefringence detection processing routes are followed:
A) Azimuthal slowness detection scan over the Rn array interval only (~ 1m), independently for VS-fast and VS-slow
B) Conventional-Alford-Esmersoy type, 4 x Rn signal response detection between source and mid array positions (~ 3m)

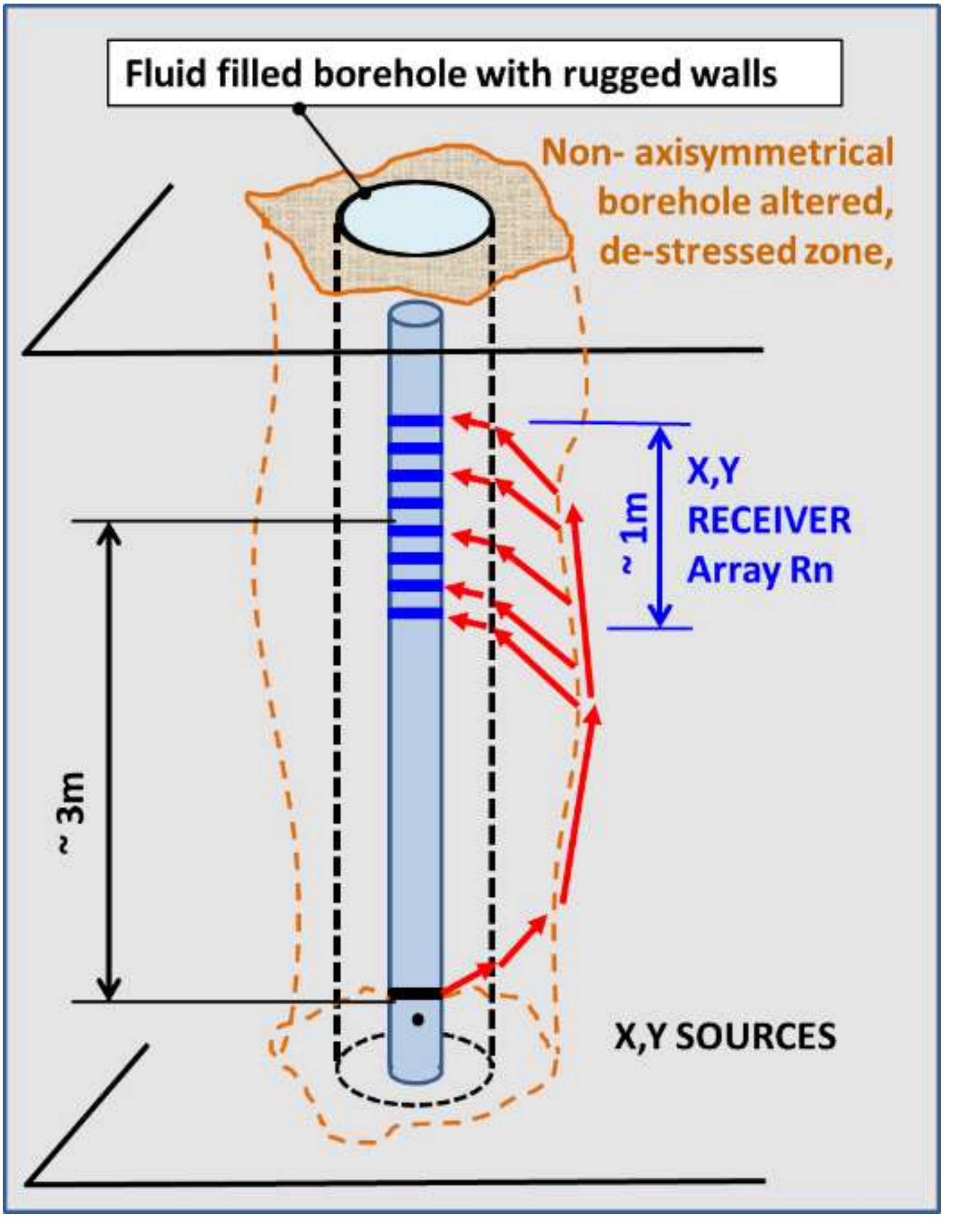

Dipole Array Sonic tool in the borehole

Fig I-4

TWO birefringence detection processing routes are followed:
A) Azimuthal slowness detection scan over the Rn array interval only (~ 1m), independently for VS-fast and VS-slow
B) Conventional-Alford-Esmersoy type, 4 x Rn signal response detection between source and mid array positions (~ 3m)

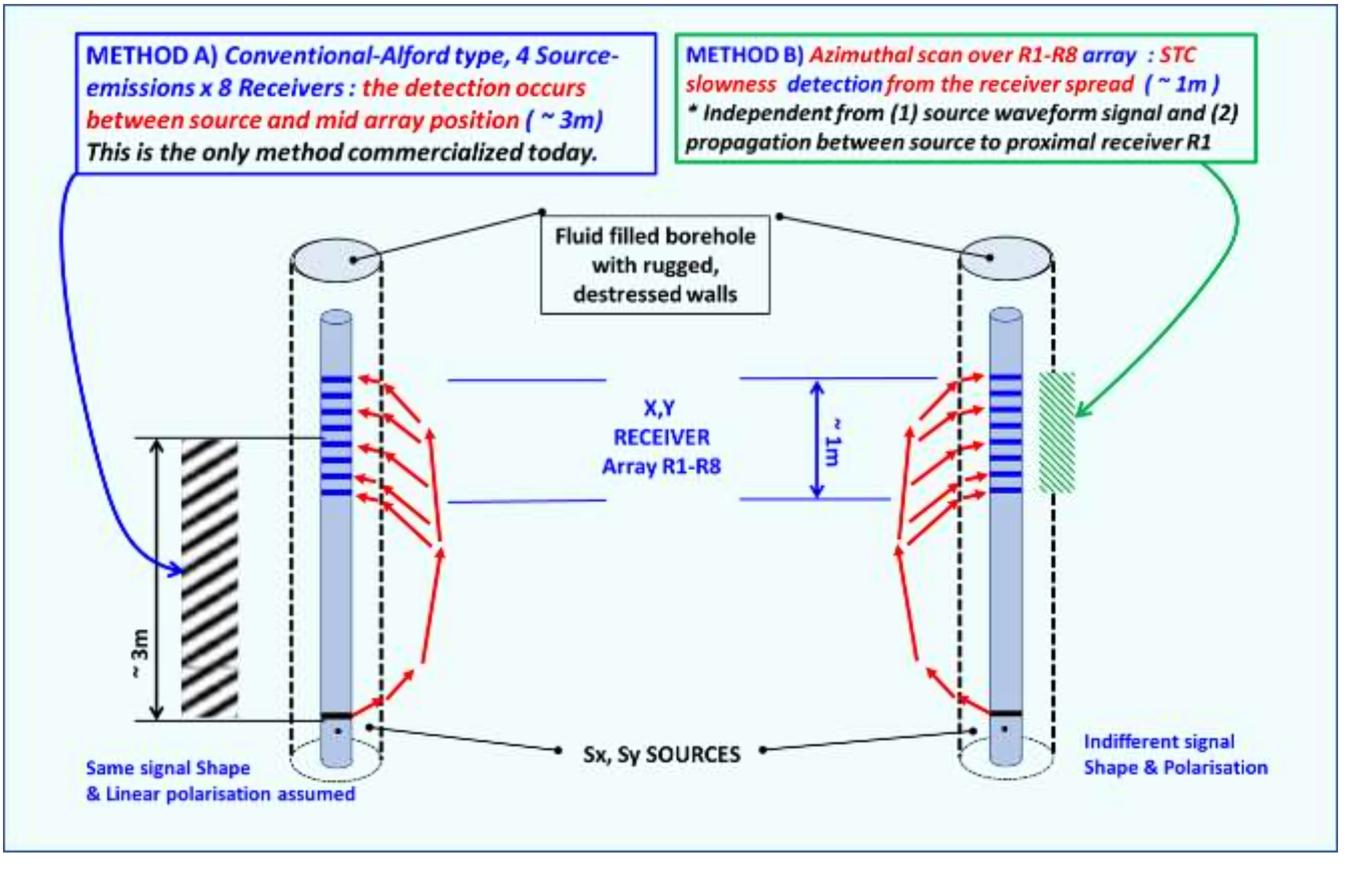

SPWLA-France workshop on Acoustics, March 31st at SGF_PARIS
Presentation by Charles Naville, IFPEN; 14h30-15h ; **DSI Anisotropy**
PART-2: Case study # 1: GDF – France (now STORENGY)

Vertical well, low structural dip; Open Hole dipole sonic runs

Initial dipole sonic data processing results were obtained in 1992
by **JP Yver & D. Belaud, SCHLUMBERGER- France,**
in behalf of **Frederic Huguet , GDF (now STORENGY, France),**
as a prototype S-wave splitting detection approach.

Computing the S-wave STC slowness every 15° in azimuthal increment, after rotating the source in the same direction of the inline receivers, was considered by the authors as the most appropriate method to apply for birefringence detection.
STC acquisition = 4 levels of (X,Y) sensors recorded simultaneously for each EX, then EY source activations (2 records)

In parallel, in the early 1990's, C. Esmersoy, M. Kane & al., SCHLUMBERGER-USA were entrusted with developing an S-wave dection method, based on *minimisation of the cross-dipole energy for the flexural S-wave propagation between dipole sources and the receiver array. They chose to work on the BCR records.*
BCR acquisition = 8X, then 8Y sensors recorded simultaneously for each EX, then EY source activations (4 records)

The results from the two methods (following slides), show notable differences, better understood today, however due to different different S-wave propagation assumptions.

Rotation-Scan results: **Fig II-1**

DTS-max and DTS-min slownesses have been computed and displayed. The Fast-S Azimuth was NOT sorted

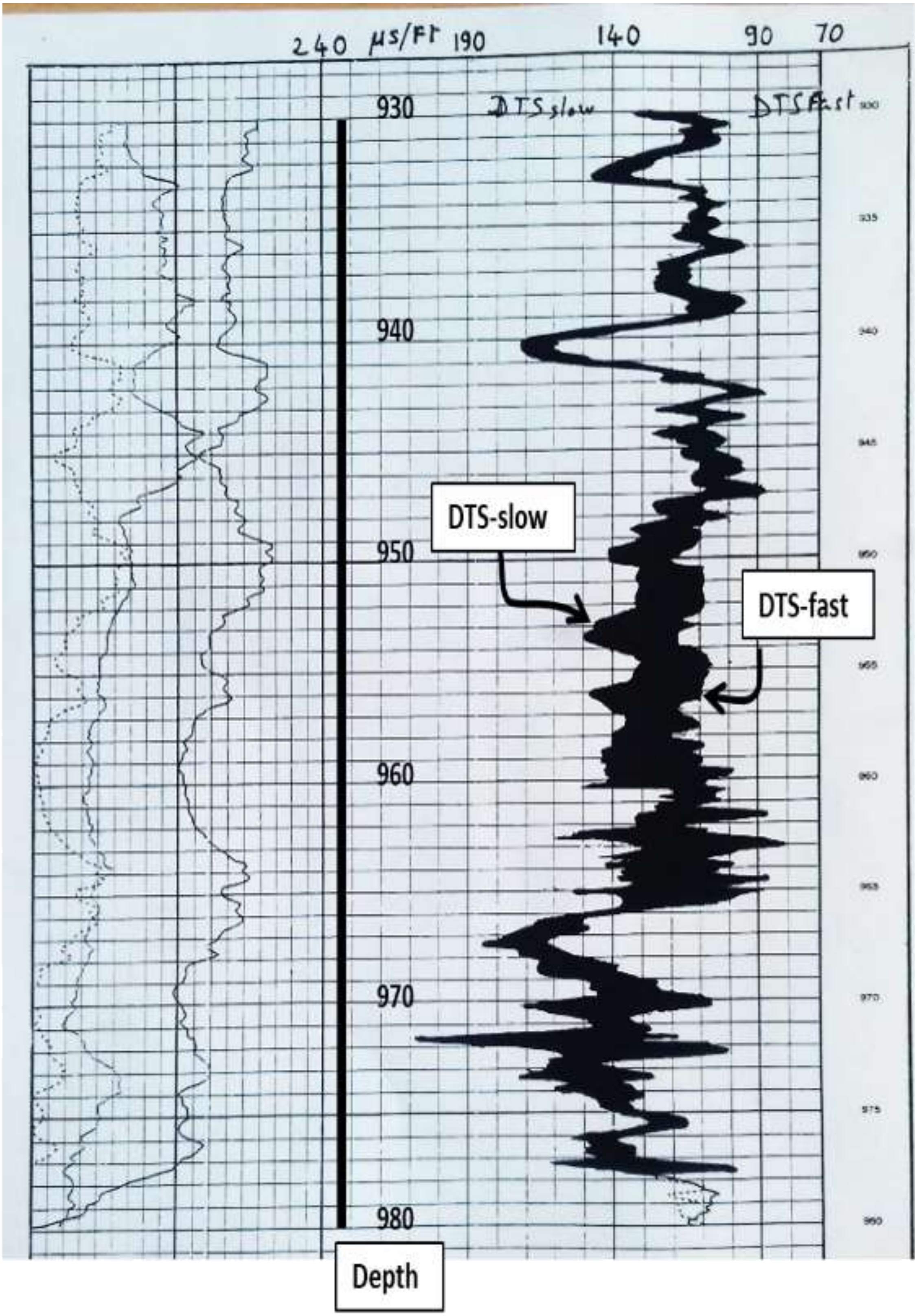

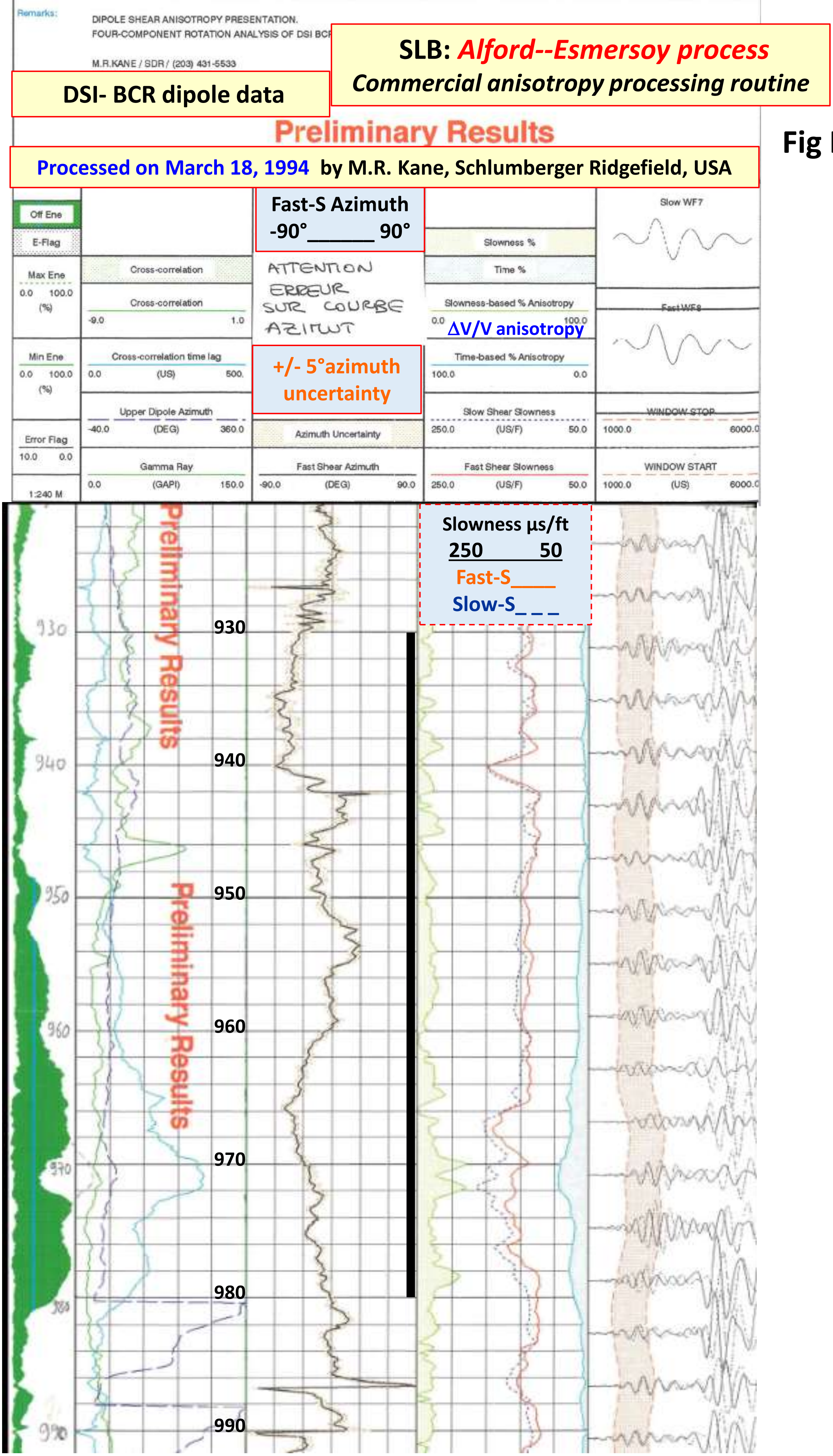
Remarks:
DIPOLE SHEAR ANISOTROPY PRESENTATION.
FOUR-COMPONENT ROTATION ANALYSIS OF DSI BCR
M.R.KANE / SDR / (203) 431-5533
DSI- BCR dipole data
SLB: Alford--Esmersoy process
Commercial anisotropy processing routine
Preliminary Results
Processed on March 18, 1994 by M.R. Kane, Schlumberger Ridgefield, USA
Off Ene
E-Flag
Max Ene
0.0 100.0 (%)
Min Ene
0.0 100.0 (%)
Error Flag
10.0 0.0
1:240 M
Cross-correlation
Cross-correlation
-9.0 1.0
Cross-correlation time lag
0.0 (US) 500.
Upper Dipole Azimuth
-40.0 (DEG) 360.0
Gamma Ray
0.0 (GAPI) 150.0
Fast-S Azimuth
-90° 90°
ATTENTION ERREUR SUR COURBE AZIMUT
+/- 5°azimuth uncertainty
Azimuth Uncertainty
Fast Shear Azimuth
-90.0 (DEG) 90.0
Slowness %
Time %
Slowness-based % Anisotropy
0.0 100.0
ΔV/V anisotropy
Time-based % Anisotropy
100.0 0.0
Slow Shear Slowness
250.0 (US/F) 50.0
Fast Shear Slowness
250.0 (US/F) 50.0
Slow WF7
Fast WF8
WINDOW STOP
1000.0 6000.0
WINDOW START
1000.0 (US) 6000.0
930
940
950
960
970
980
990
Preliminary Results
Preliminary Results
Slowness µs/ft
250 50
Fast-S____
Slow-S_ _ _

Fig II-2

Fig II-3

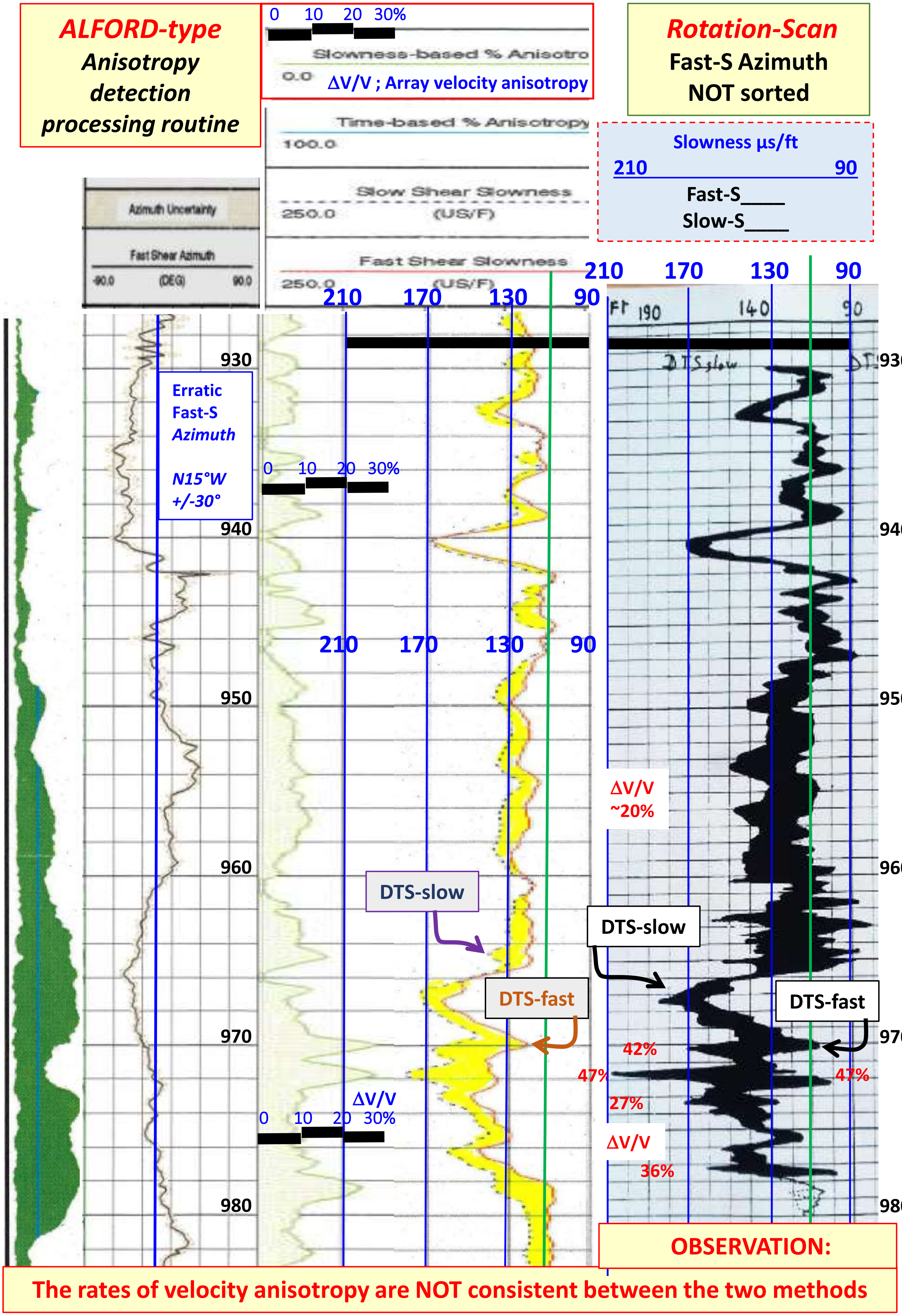

Courtesy of STORENGY- FRANCE

SPWLA-France workshop on Acoustics, March 31st at SGF_PARIS
Presentation by Charles Naville, IFPEN; 14h30-15h ; **DSI Anisotropy**
PART-3: Case study # 2: BRGM – France (Well MM-1)

Vertical well, low structural dip; Open Hole dipole sonic runs

Dipole sonic processing results
obtained in the scientific well MM-1 of BRGM, 1993
by **JP Yver & D. Belaud, SCHLUMBERGER- France,**
in behalf **of José PERRIN, BRGM**, **France),**

Computing the S-wave STC slowness every 10° in azimuthal increment, after rotating the source in the same direction of the inline receivers, was considered by the authors as the most appropriate method to apply for birefringence detection.
STC acquisition = 4 levels of (X,Y) sensors recorded simultaneously for each EX, then EY source activations (2 records)

In parallel, in the early 1990's, C. Esmersoy, M. Kane & al., SCHLUMBERGER-USA were entrusted with developing an S-wave dection method, based on *minimisation of the cross-dipole energy for the flexural S-wave propagation between dipole sources and the receiver array. They chose to work on the BCR records.*
BCR acquisition = 8X, then 8Y sensors recorded simultaneously for each EX, then EY source activations (4 records)

The results from the two methods (following slides), show notable differences due to different S-wave propagation assumptions.

Ref: ***S-wave anisotropy from two dipole sonic data processing methods, confronted with fracture permeability, logs and cores, Science and Technology for Energy Transition 77, 13 (2022); STET 210270,*** https://doi.org/10.2516/stet/2022006

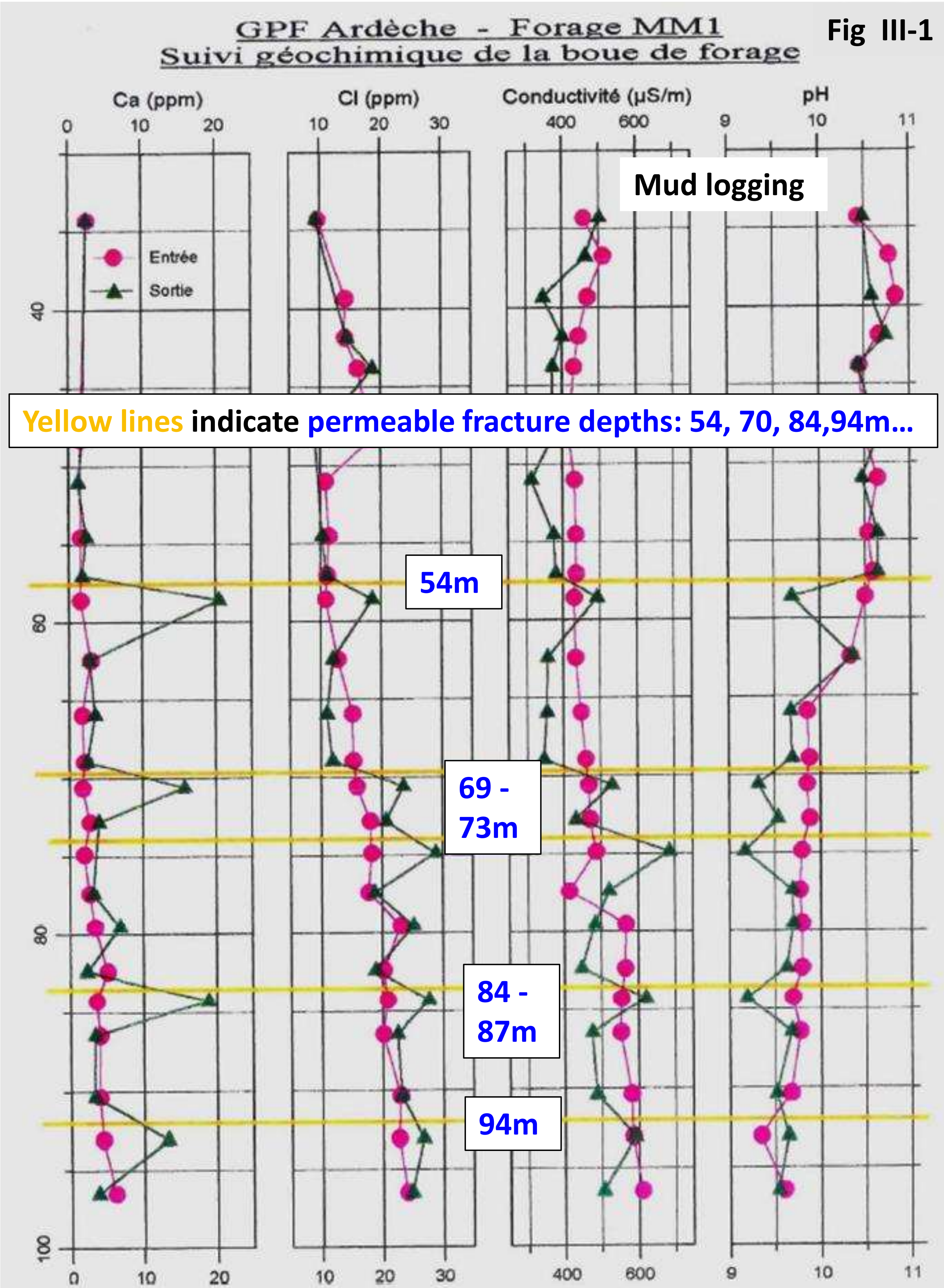
Fig III-1
GPF Ardèche - Forage MM1
Suivi géochimique de la boue de forage
Ca (ppm)
Cl (ppm)
Conductivité (µS/m)
pH
Mud logging
Entrée
Sortie
Yellow lines indicate permeable fracture depths: 54, 70, 84,94m…
54m
69 - 73m
84 - 87m
94m

Fig III - 2

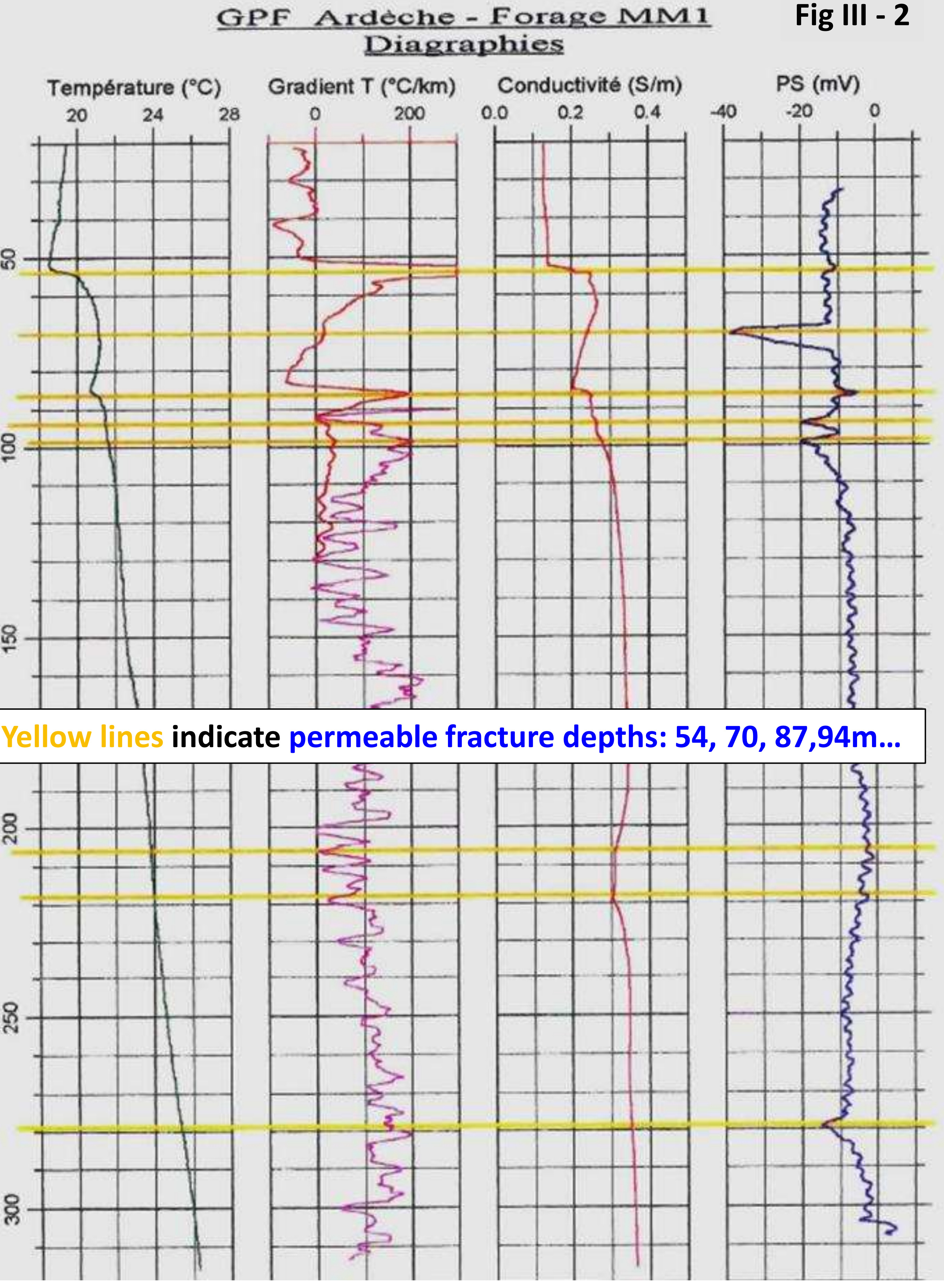
GPF Ardèche - Forage MM1
Diagraphies
Température (°C)
20
24
28
Gradient T (°C/km)
0
200
Conductivité (S/m)
0.0
0.2
0.4
PS (mV)
-40
-20
0
50
100
150
200
250
300
Yellow lines indicate permeable fracture depths: 54, 70, 87,94m…

MM-1 well: S-velocity anisotropy from Rotation-scan Fig III - 3

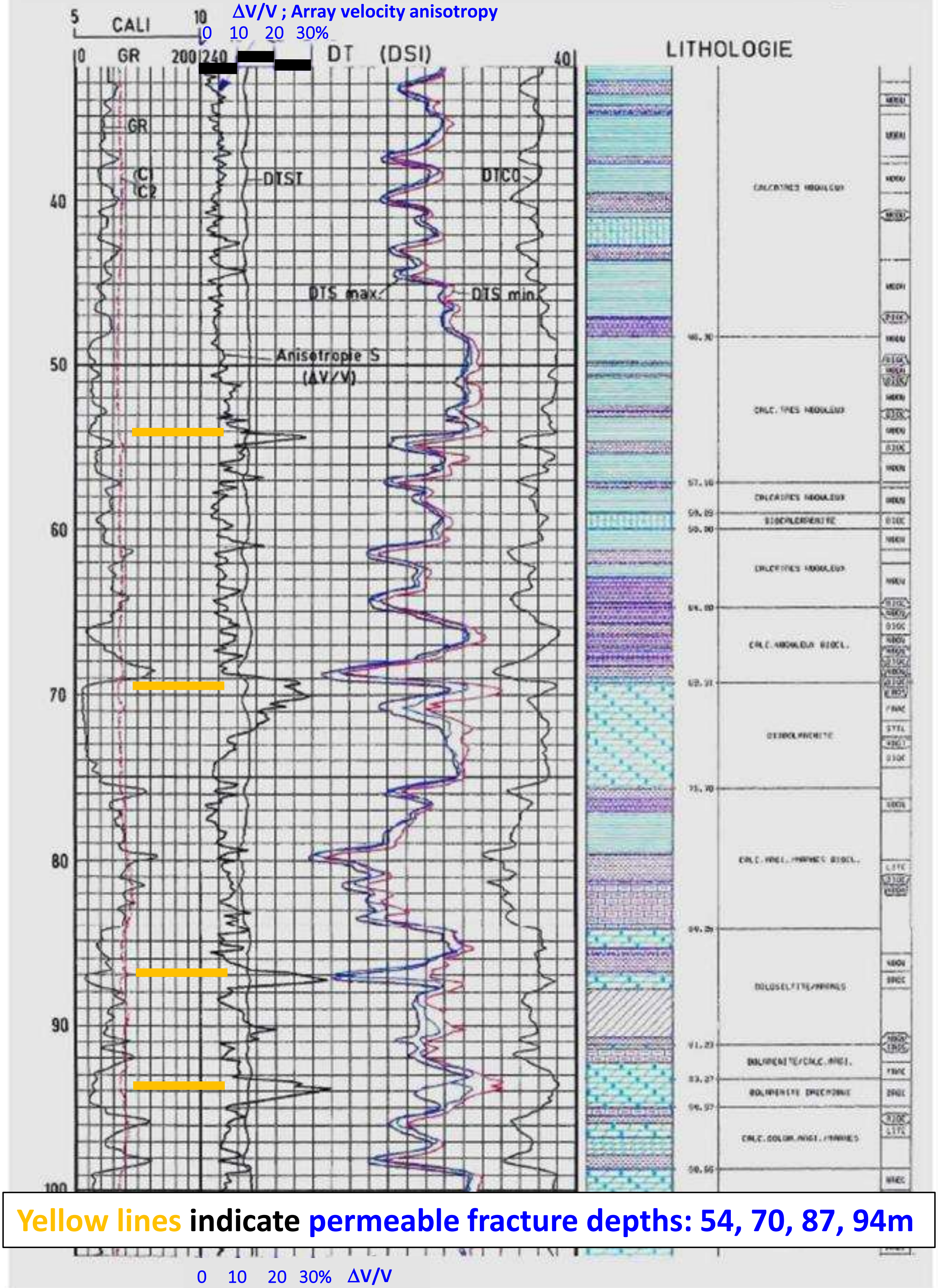

Yellow lines indicate permeable fracture depths: 54, 70, 87, 94m

Fig III - 4

FMS image of permeable fractures

Periphotographs (i.e. wrap around photos) of core external wall

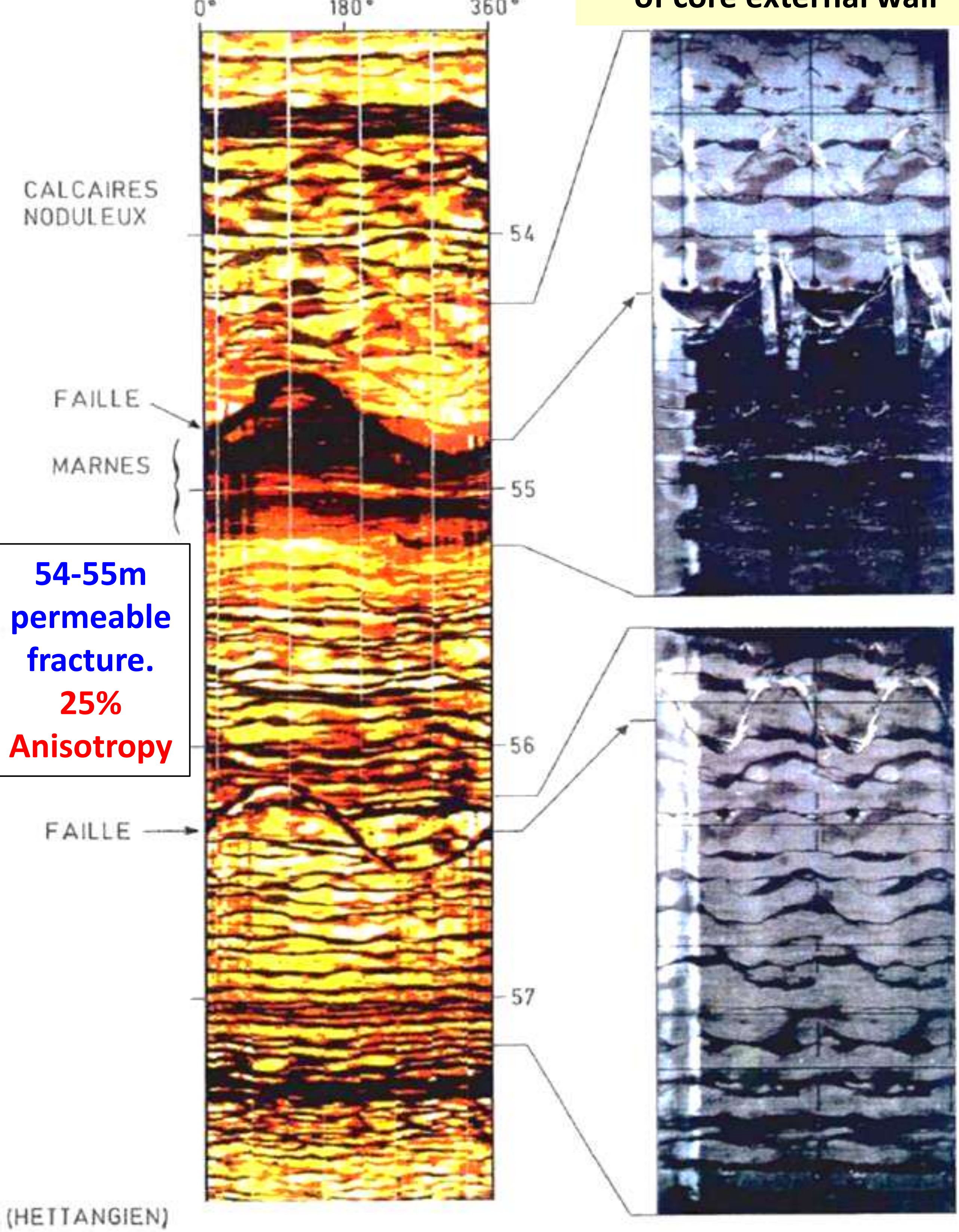

54-55m permeable fracture. 25% Anisotropy

Fig III - 5

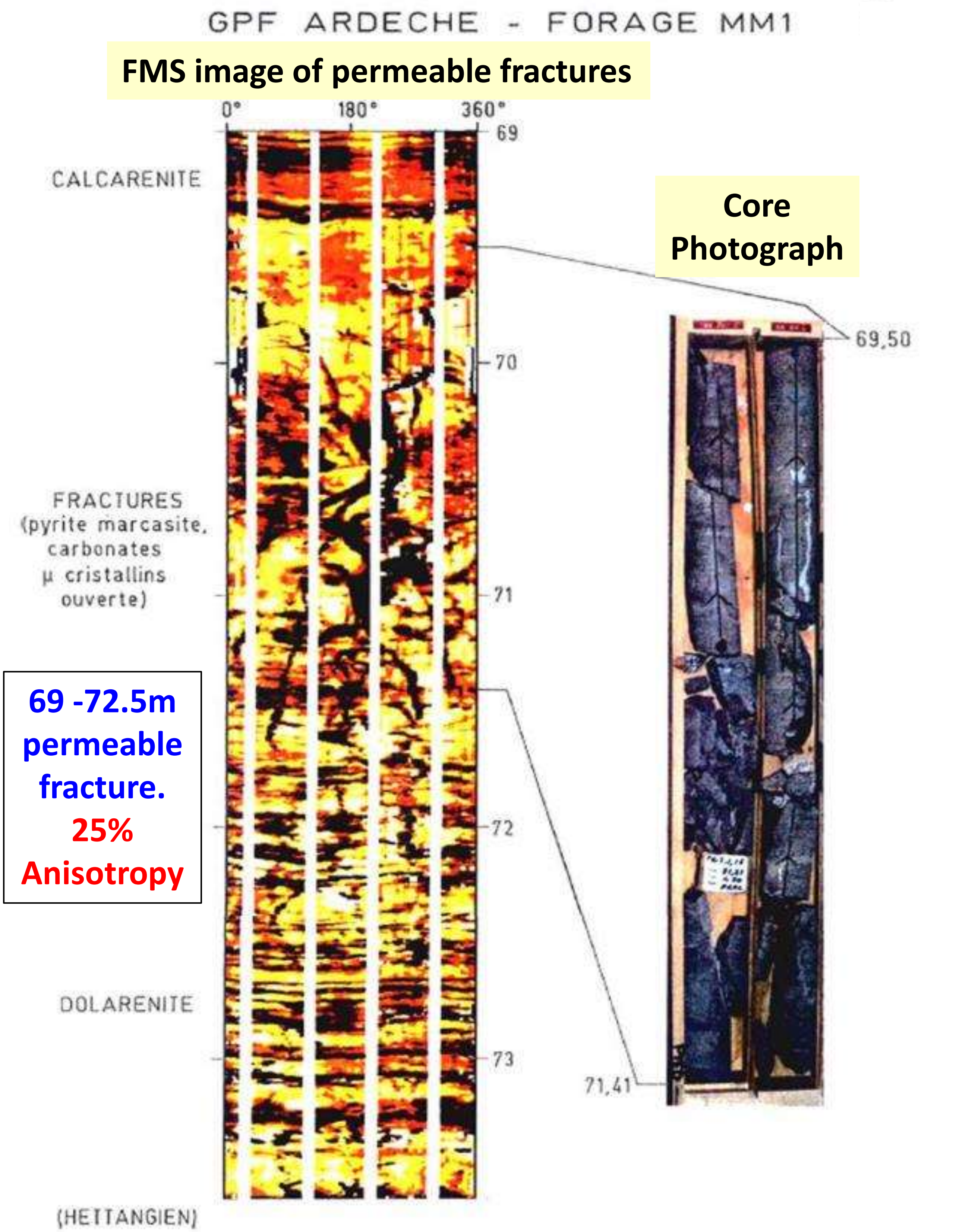
GPF ARDECHE - FORAGE MM1
FMS image of permeable fractures
0°
180°
360°
69
70
71
72
73
CALCARENITE
FRACTURES
(pyrite marcasite,
carbonates
µ cristallins
ouverte)
DOLARENITE
(HETTANGIEN)
Core
Photograph
69,50
71,41
69 -72.5m
permeable
fracture.
25%
Anisotropy

Fig III - 6

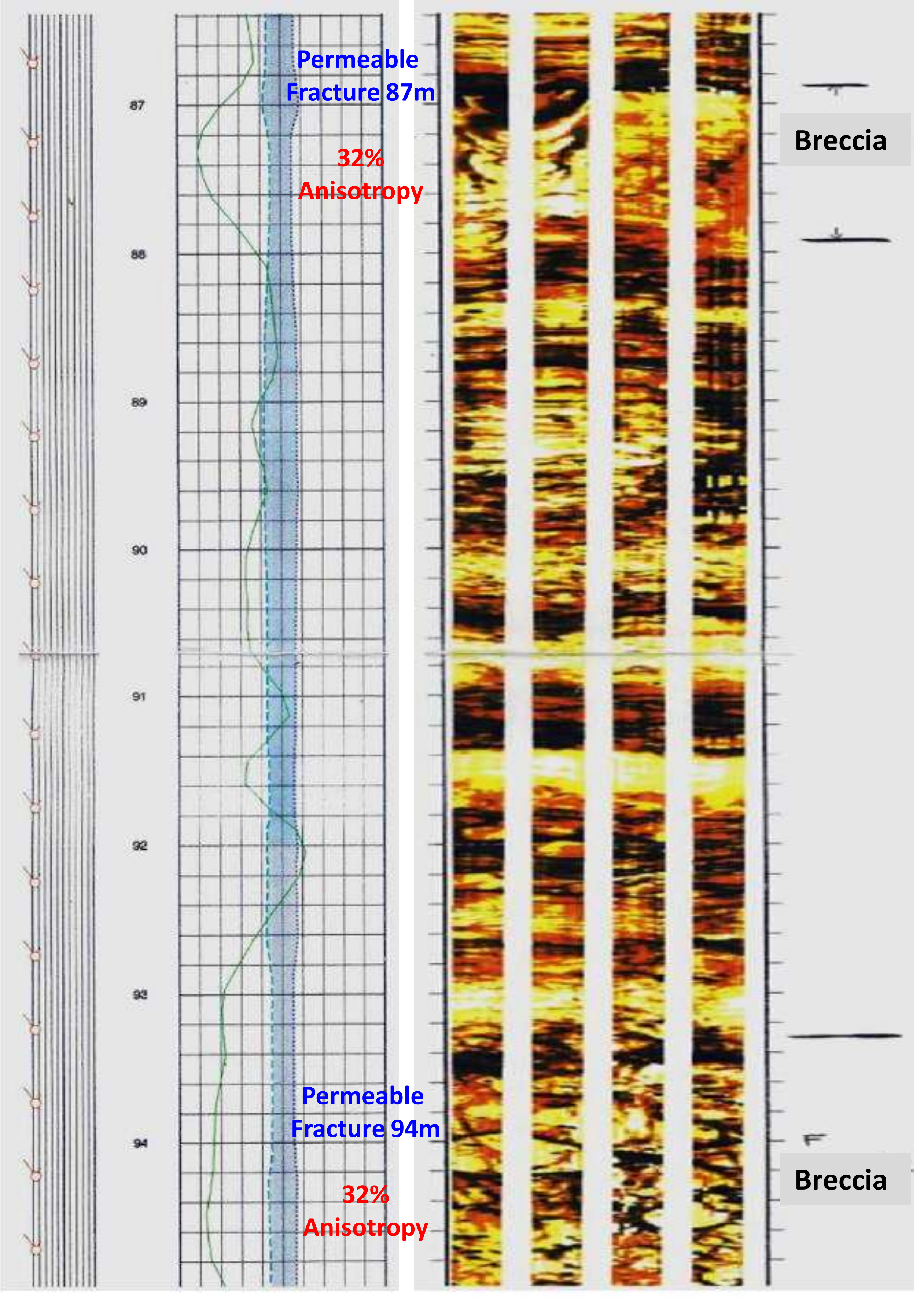
87
88
89
90
91
92
93
94
Permeable Fracture 87m
32% Anisotropy
Permeable Fracture 94m
32% Anisotropy
Breccia
Breccia

Fig III - 7

GPF ARDECHE - FORAGE MM1

FMS image of Tight, NON permable fractures : 5% Anisotropy = matrix anisotropy

Photograph of core wall

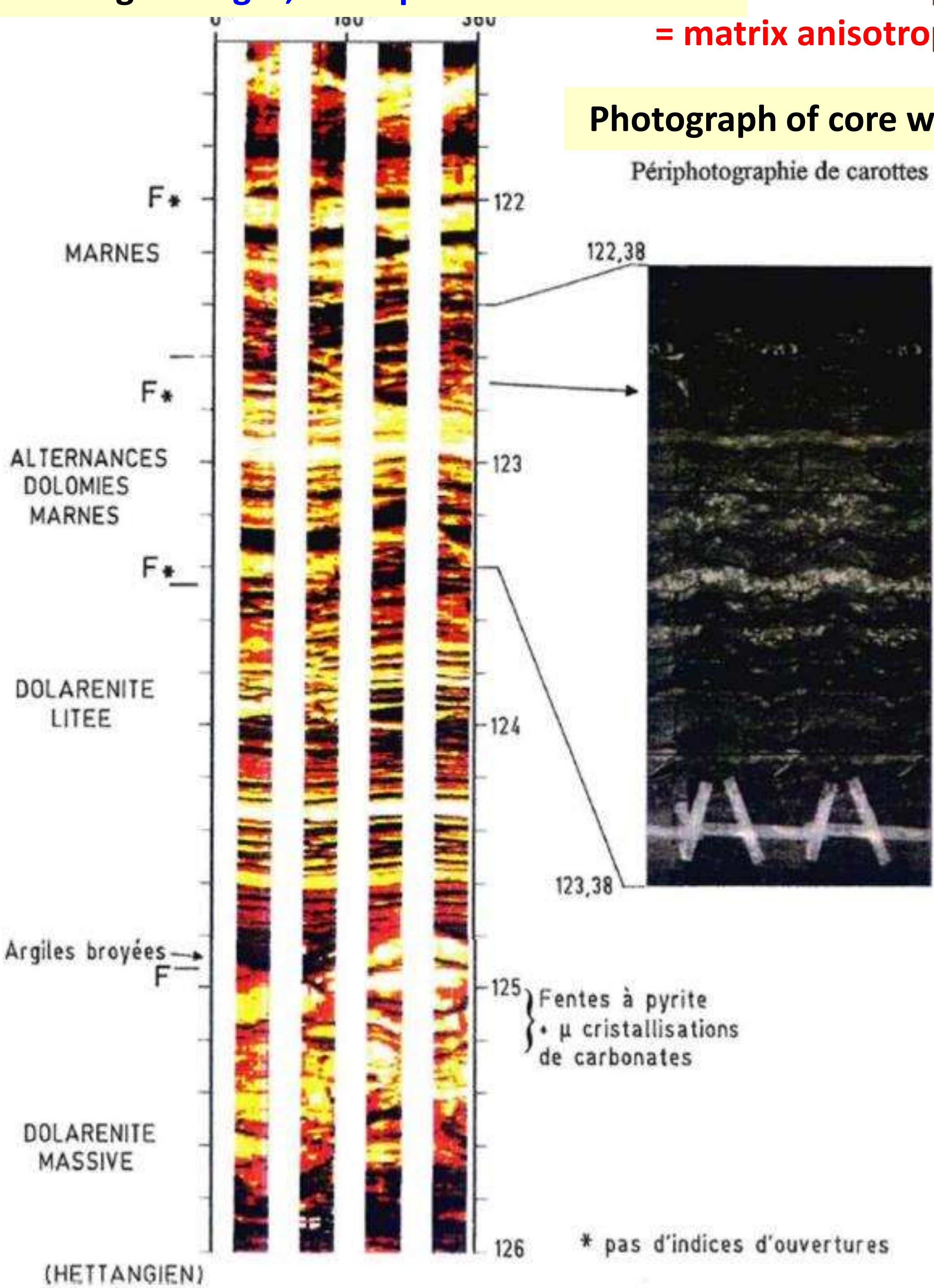

Confrontation of dipole sonic anisotropy results from both methods

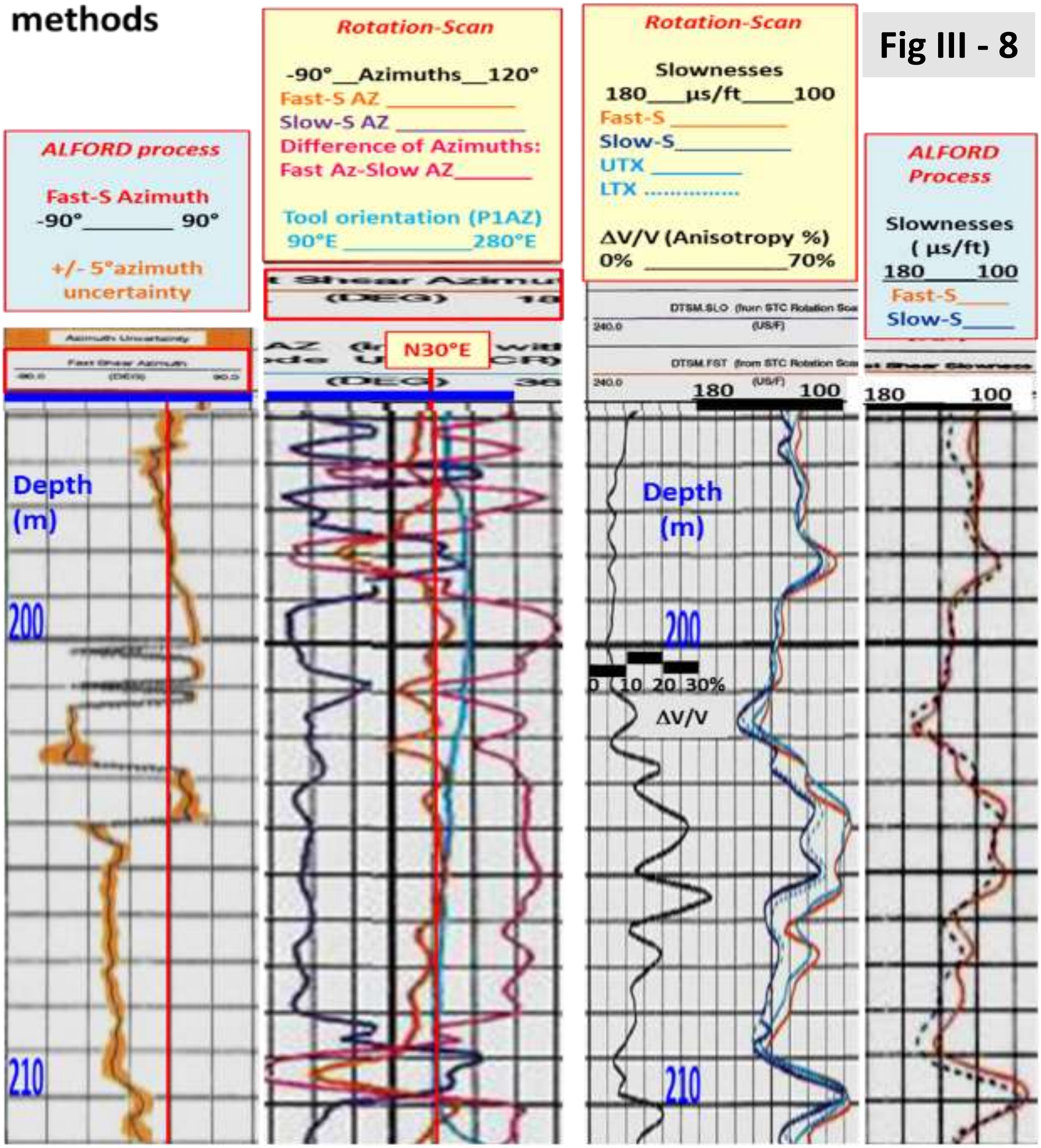

195-211m: weak Anisotropy (5%). Similar anisotropy azimuth from both methods, although Rot-scan results are more accurate. Inversion of anisotropy axes in 197.8-198.7 and 209-210m , from Rot-scan (Totally NEW result). INCORRECT to NO anisotropy detected in 202-209m interval by Alford method, versus stable birefringence azimuth and large anisotropy (10-30%) from Rot-scan

Figure 21b1: MM1 anisotropy results from both detection methods, same scale displays, depth interval 195-210m

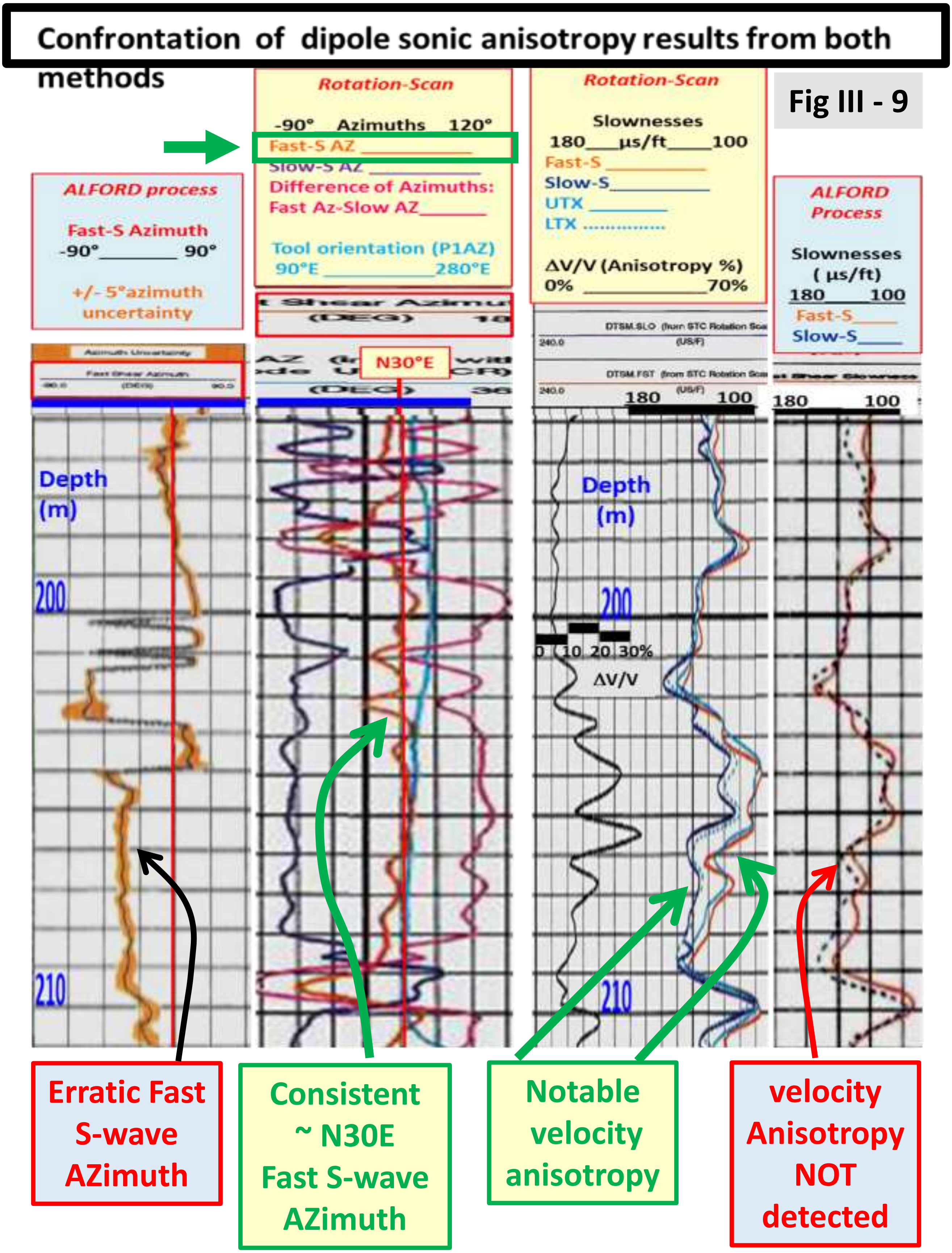

Figure 21b2: MM1 anisotropy results from both detection methods, same scale displays, depth interval 195-210m

Confrontation of dipole sonic anisotropy results from both methods

Fig III - 10

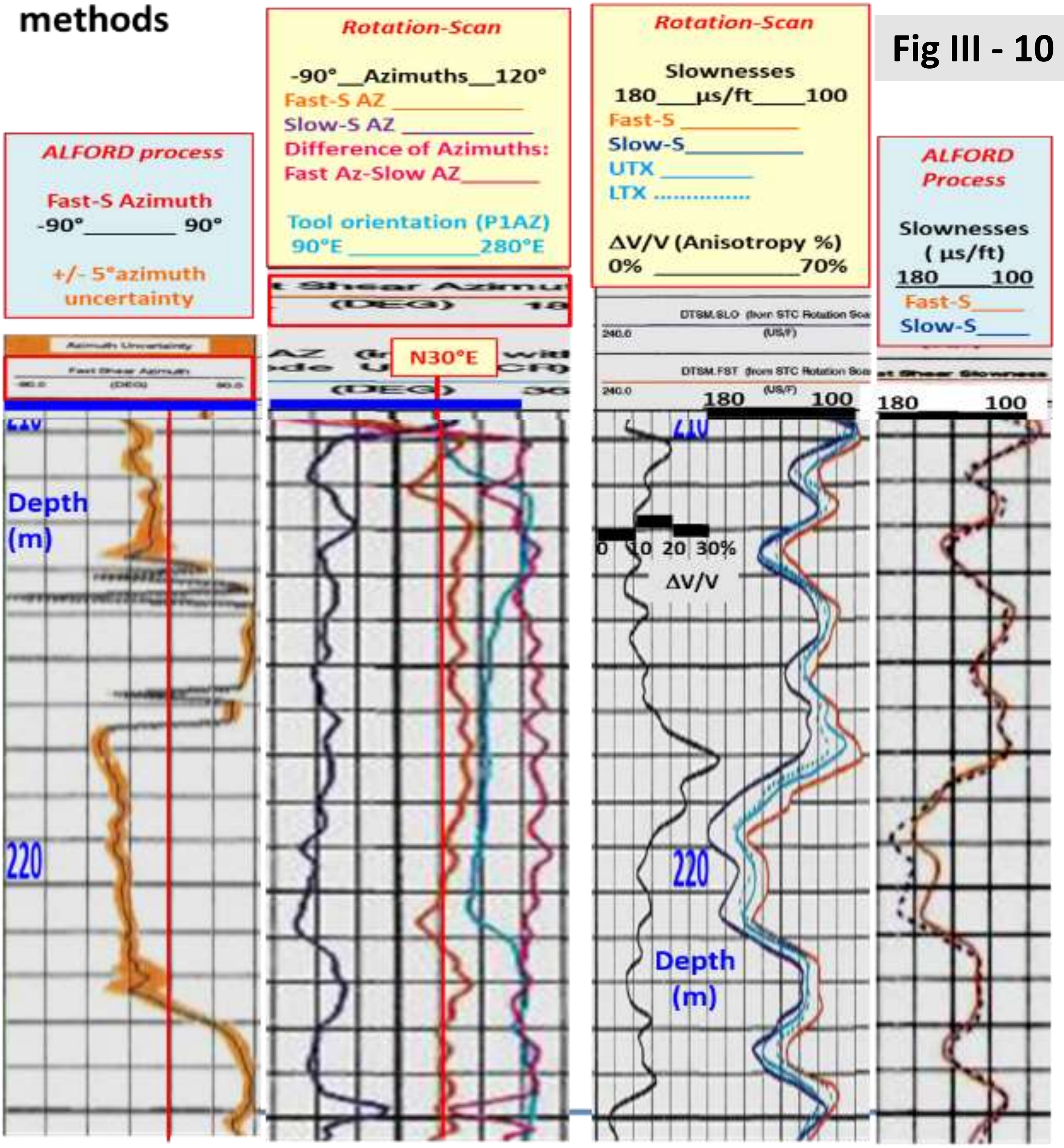

210-224m: HIGH to SUPER HIGH velocity Anisotropy (10%-30%) :

- Alford : Birefringence azimuth and anisotropy values are INCORRECT or UNDETECTED.
- Rot-scan : Stable S-fast birefringence azimuth in full agreement with local fault strike and Max. H-Stress. Independently determined principal S-waves azimuths are orthogonal (+/-10°)

Figure 21c1: MM1 anisotropy results from both detection methods, same scale displays, depth interval 210-224m

Confrontation of dipole sonic anisotropy results from both methods

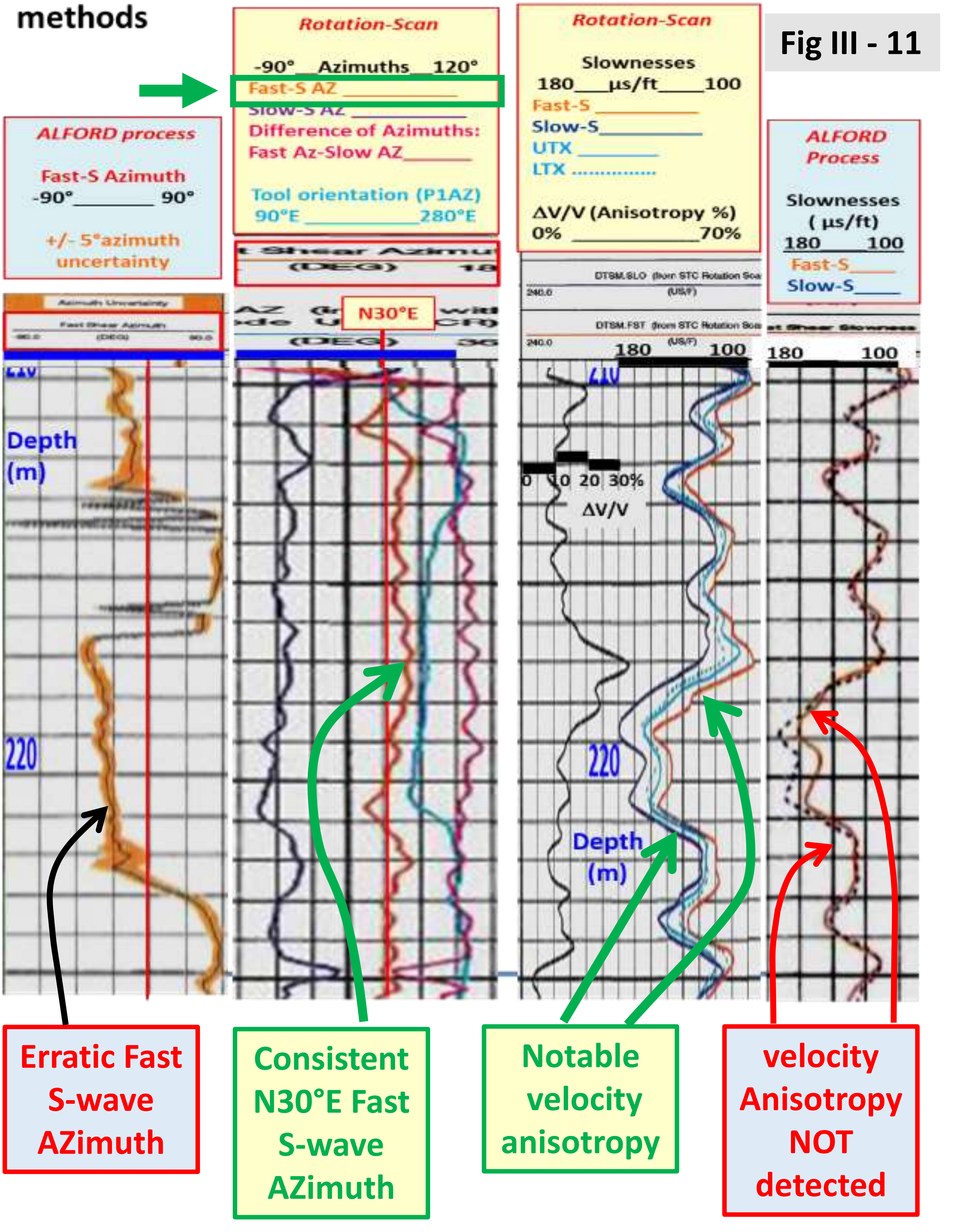

Figure 21c2: MM1 anisotropy results from both detection methods, same scale displays, depth interval 210-224m

GPF ARDECHE - Structural Sketch

Fig III - 12

2D seismic profiles (dashed lines)
Borehole location – BA1 & MM1

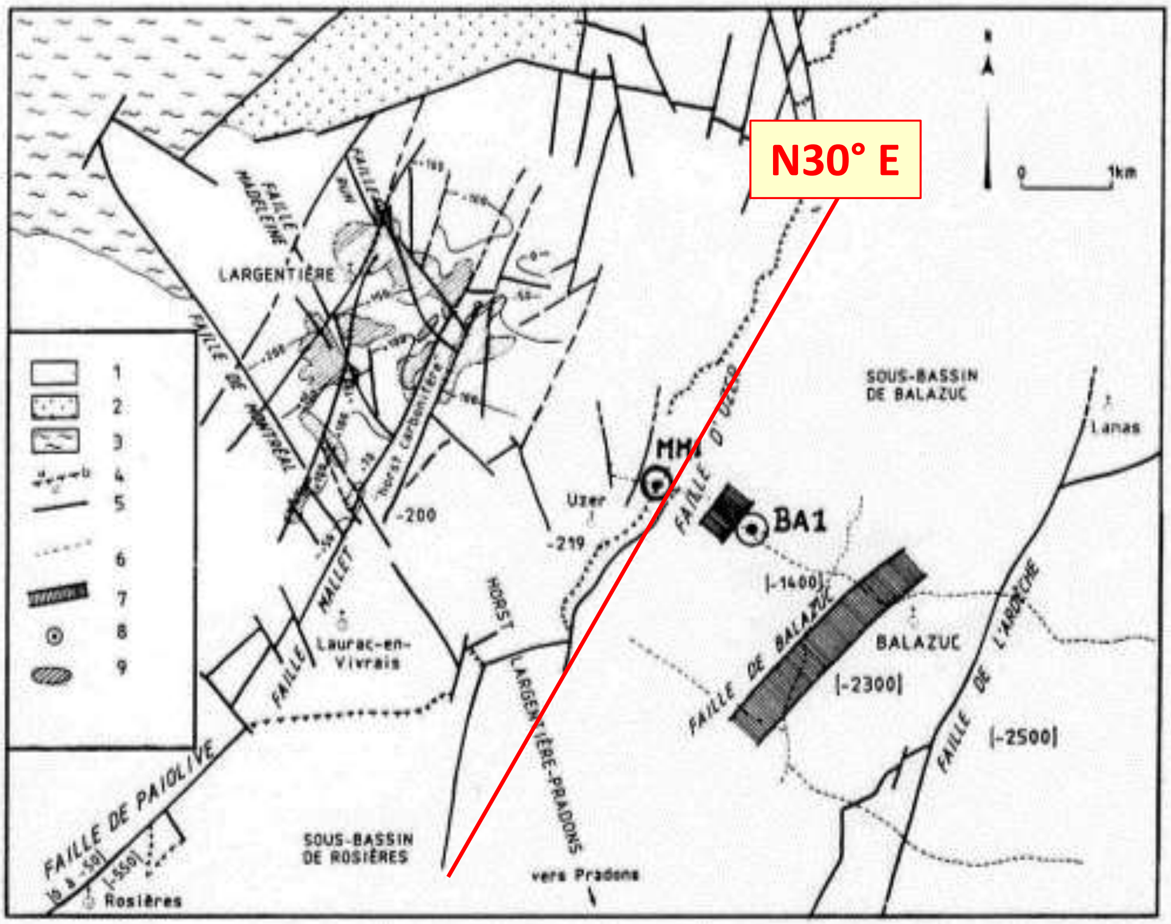

Légende: (1) Couverture sédimentaire mésozoïque, (2) Permien, (3) Socle, (4) Paléosurface à sédimentation réduite, (5) Failles observée, (6) Profils sismiques GPF, (7) Failles décélées par la sismique, (8) Forages GPF, (9) Amas sulfurés de Largentière

The N30°E Fast S-wave azimuth (FAZ) from dipole sonic matches the strike of the neighboring Uzer Fault

Figure 2 : GPF ARDECHE - Schéma structural - Localisation des forages

Two birefringence detection processing routes

Fig III - 13

	Alford-type method T-R ANI (Algorithm-1)	Azimuthal DTS Rotation-Scan Array ANI (Algorithm2)
PRINCIPLE	Minimizing cross dipole energy, or Minimizing the off-diagonal elements of the 4-term matrix of the Source(s) to Receiver(r) signals (XsXr, XsYr, YsXr, YsYr).	Scan of S-wave slowness/velocity over 180° azimuth range, to *INDEPENDENTLY* determine the azimuths of Vs-max & Vs-min
ASSUMPTIONS	The propagation medium between Transmitter to the Receiver array is considered homogeneous, with same anisotropy axes, possibly stratified axisymmetric.	The propagation medium is considered homogeneous over the Receiver array ONLY. The SHORT detection interval yields a higher depth resolution
	Emitted flexural S-wave particle motion **remains LINEAR** in the borehole formation located in the immediate source vicinity. Equal orthogonally emitted signals, in same shape , same amplitude	**No polarization constraint:** Emitted S-wave imparted into the formation **can be in any form, LINEAR, ELLIPTICAL, CIRCULAR…** Orthogonally emitted signals may be a bit different.
For BOTH methods:	The borehole ruggedness and heterogeneous borehole altered zone over the detection depth interval may alter the accuracy of results	
	Differential attenuation (QDs) between the two principal S-wave modes is **NOT considered**	When NO velocity anisotropy is detected, a scan of S-wave attenuation **(Att-Rot-Scan)** versus azimuth can be run to yield the **S-wave attenuation anisotropy &** the Differential attenuation **(QDs)**
Observed RESULTS	Fast-S-wave Azimuth is searched FIRST, resulting in INACCURATE to FALSE principal S-wave principal azimuths when hypotheses are unsatisfied, or in case of weak S-wave anisotropy.	Fast-S-wave Azimuth is derived from the azimuthal STC slowness scan, resulting in higher azimuth accuracy of principal S-wave modes, and higher depth resolution. STC routine could be improved where the receiver array is located over a strong velocity contrast.
	The borehole ruggedness and heterogeneous borehole altered zone over the detection depth interval may alter the accuracy of results, The larger the detection interval, the larger potential bias…	

TABLE 1: Comparison of S-wave birefringence detection methods

DIPOLE SONIC BIREFRINGENCE DETECTION

WAY FORWARD

Fig III - 14

ex: application of both detection methods on the SAME DSI dataset recording cycle

by Tom BRATTON, Litteton, CO, USA
tom@tombrattonllc.com

FORGE dataset DSST tool (latest DSI) in BCR recording mode

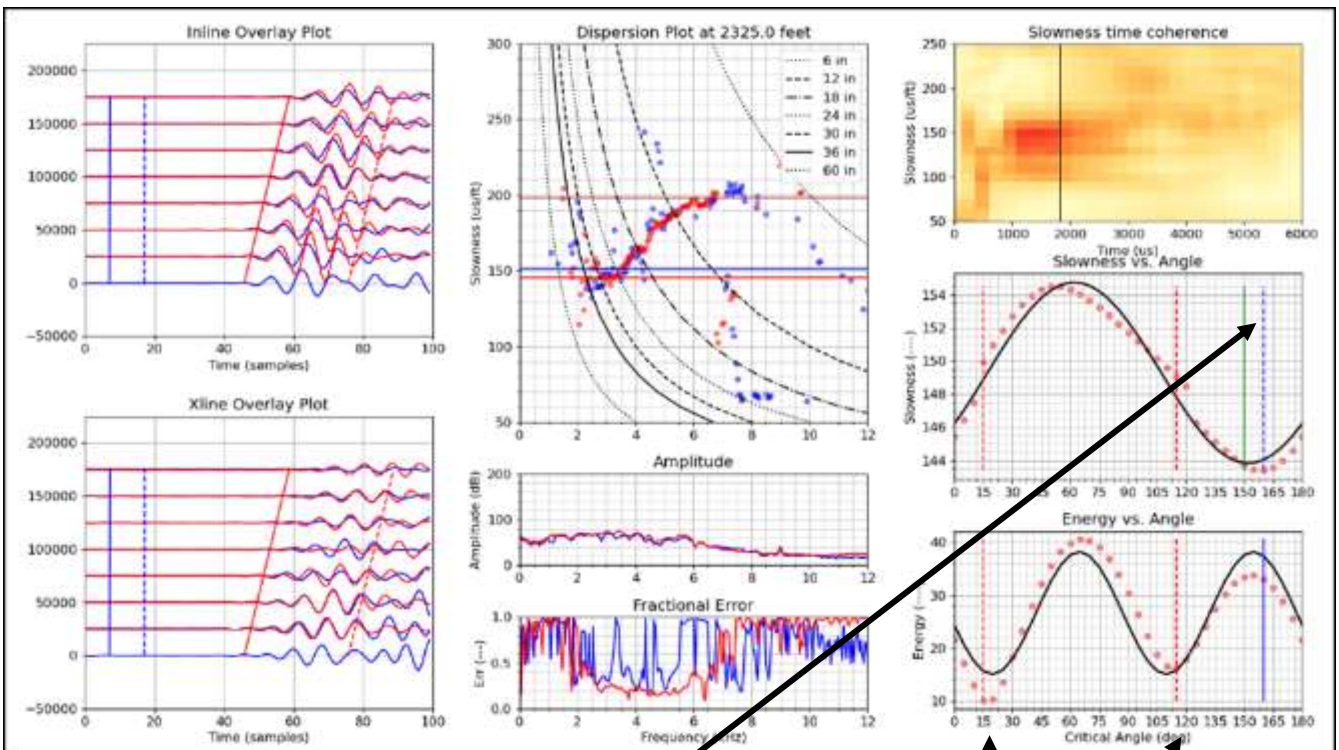

Rot-scan plot; STC slowness scan vs Azimuth
The minimum STC S-wave slowness occurs in azimuth of 157° (dashed blue line)

Alford-Esmersoy result plot: Cross line Energy vs Azimuth
The minimum Cross line Energy appear along Azimuths 15° and 115° (dashed red lines)

Fig III - 15

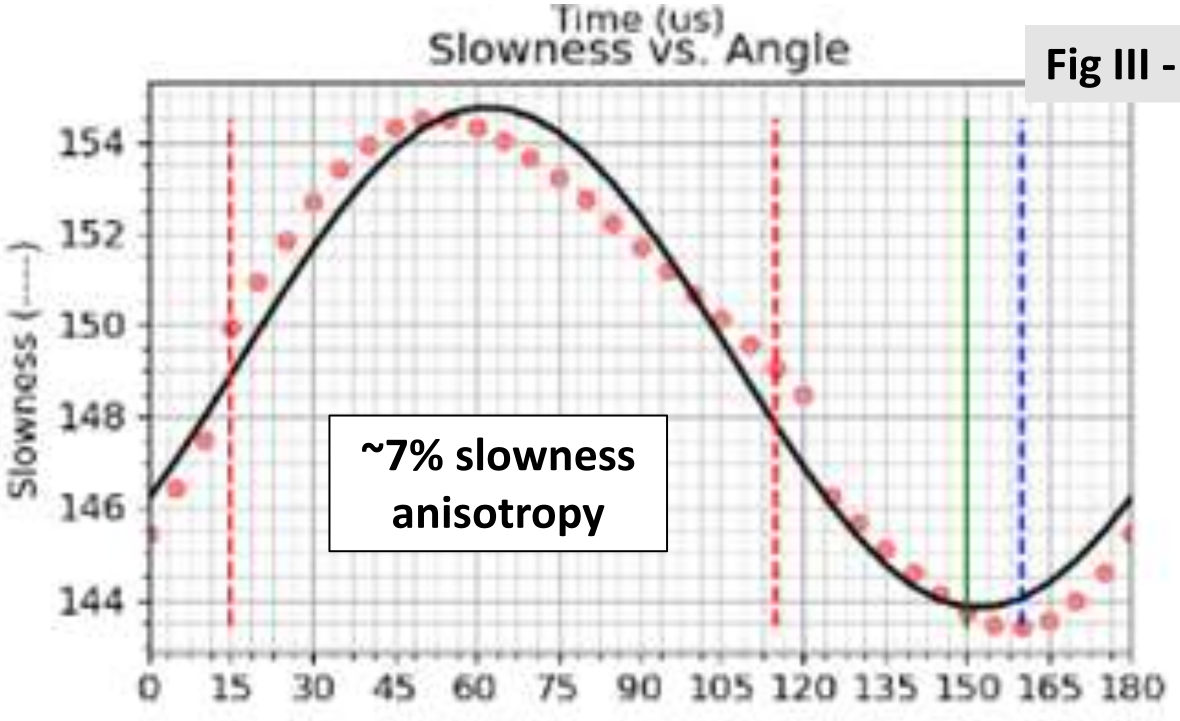

Rot-scan plot; STC slowness scan vs Azimuth
The minimum STC S-wave slowness occurs in azimuth of 157° (dashed blue line), regularized at 150° using a sine curve regression (solid green line)

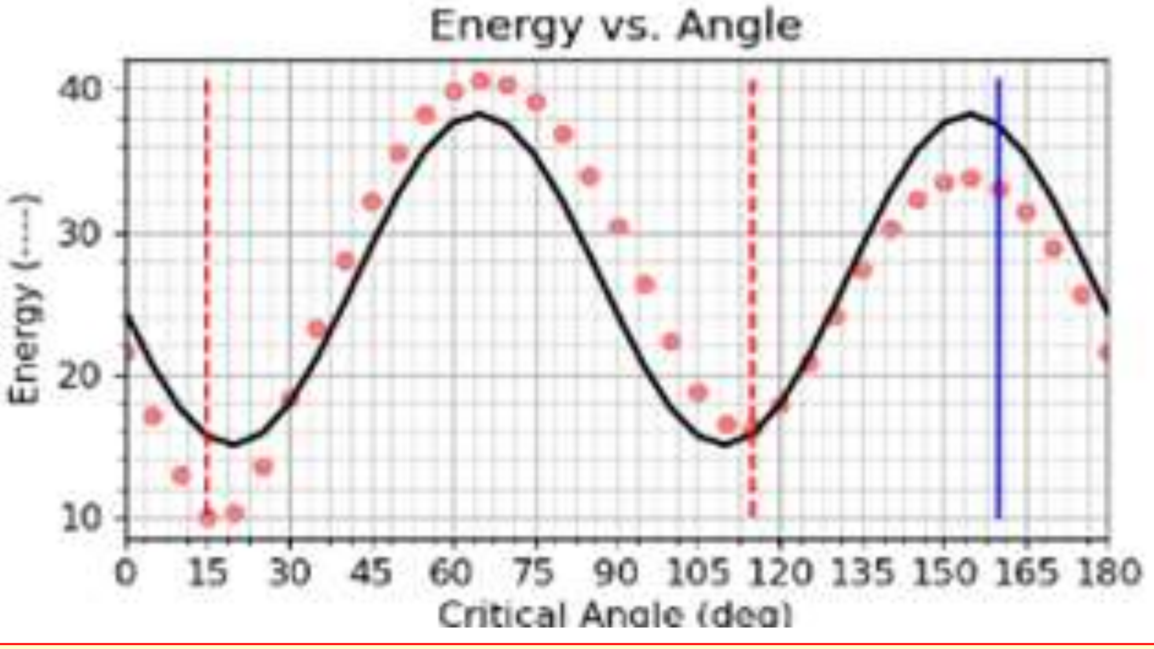

Alford-Esmersoy result plot: Cross line Energy vs Azimuth
The minimum Cross line Energy appear along Azimuths 15° and 115° (dashed red lines).
The above example shows major discrepancies, indicating a violation of the S-wave propagation assumptions. (Improvement ongoing)

Borehole geometry explanation for dipole sonic result difficulties and discrepancies

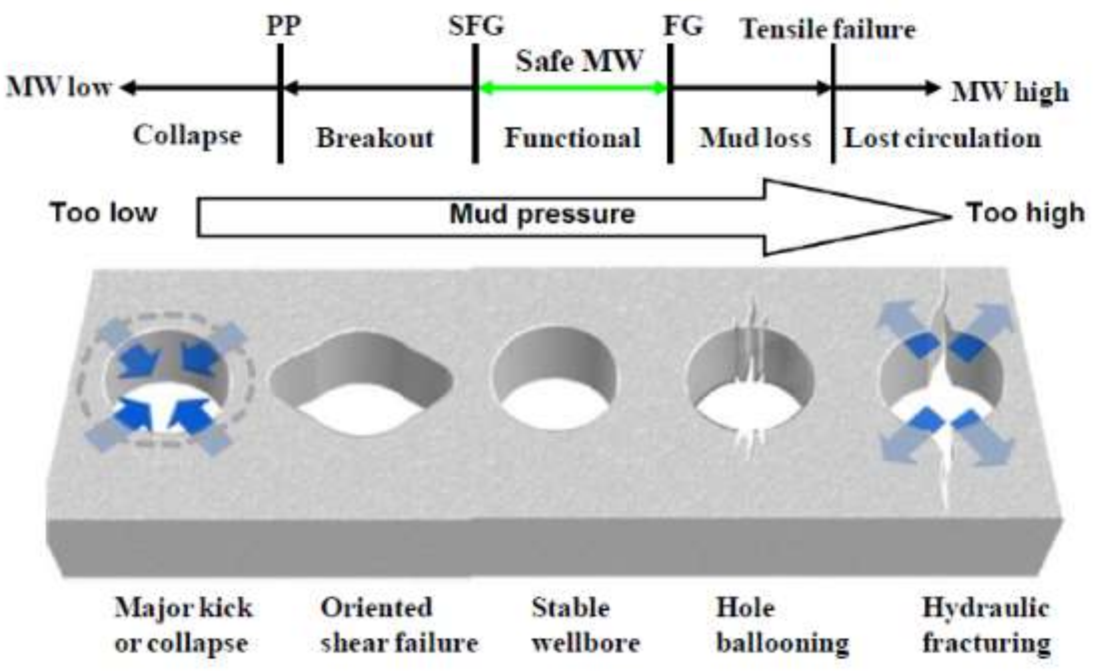

Schematic relationship of mud pressure (mud weight) and borehole failure, reproduced from Figure 1 of Zhang J. 2013: Borehole stability analysis accounting for anisotropies in drilling to weak bedding planes. International Journal of Rock Mechanics and Mining Sciences, Volume 60, June 2013, Pages 160-170.
https://doi.org/10.1016/j.ijrmms.2012.12.025

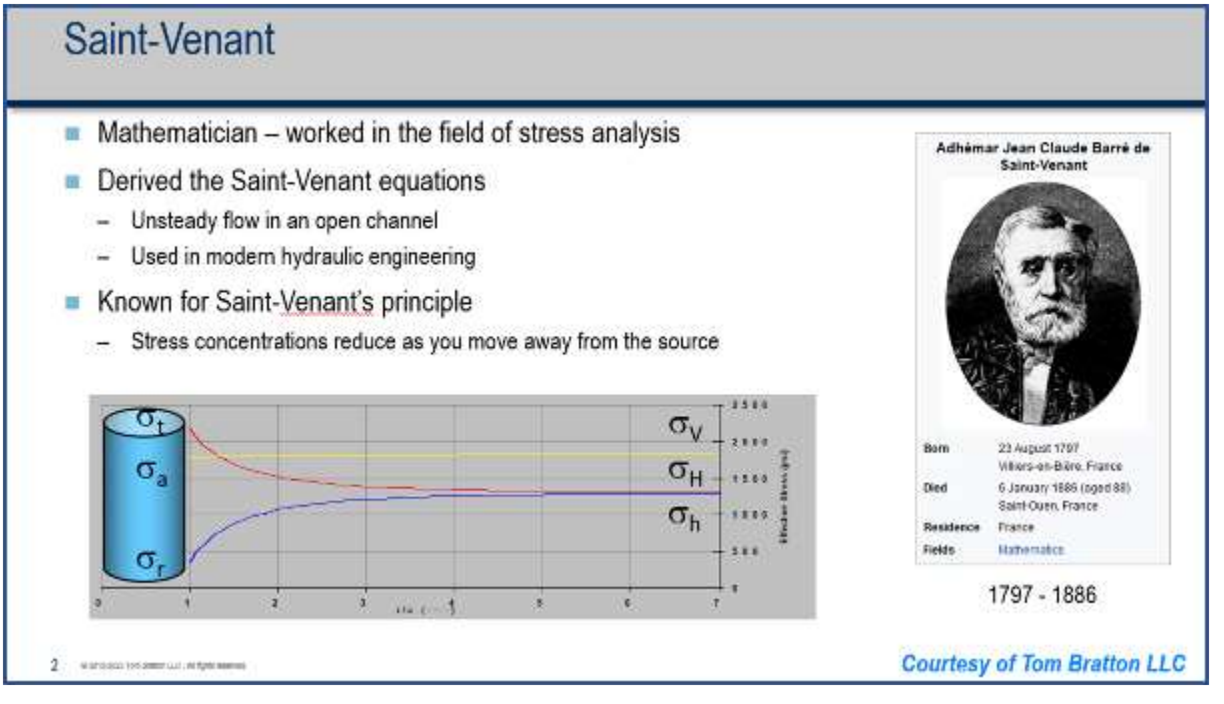

Classical geomechanics knowledge about the stress alteration around a borehole, mainly within a radial domain of three times the borehole radius. Courtesy of Tom Bratton.

SPWLA-France workshop on Acoustics, March 31st at SGF_PARIS
Presentation by Charles Naville, IFPEN; 14h30-15h ; **S-Birefringence**
PART-4: in-house Attenuation anisotropy observation

In house Shear wave test facility
on composite material samples, or rock samples,
under eventual uniaxial constraint,

Built by Bernard ZINSZNER et al., IFP- Rueil, France, 1986-1988

Ref: *Etude expérimentale de l'anisotropie dans les roches .*
Ondes ultrasonores P et S, by Miss Isabelle JONCOUR
IFP internal report # 35 997, Mars 1988

Analog in house fractured rock model **Fig IV-1**
& polarising filter @ utrasonic frequency 500kHz

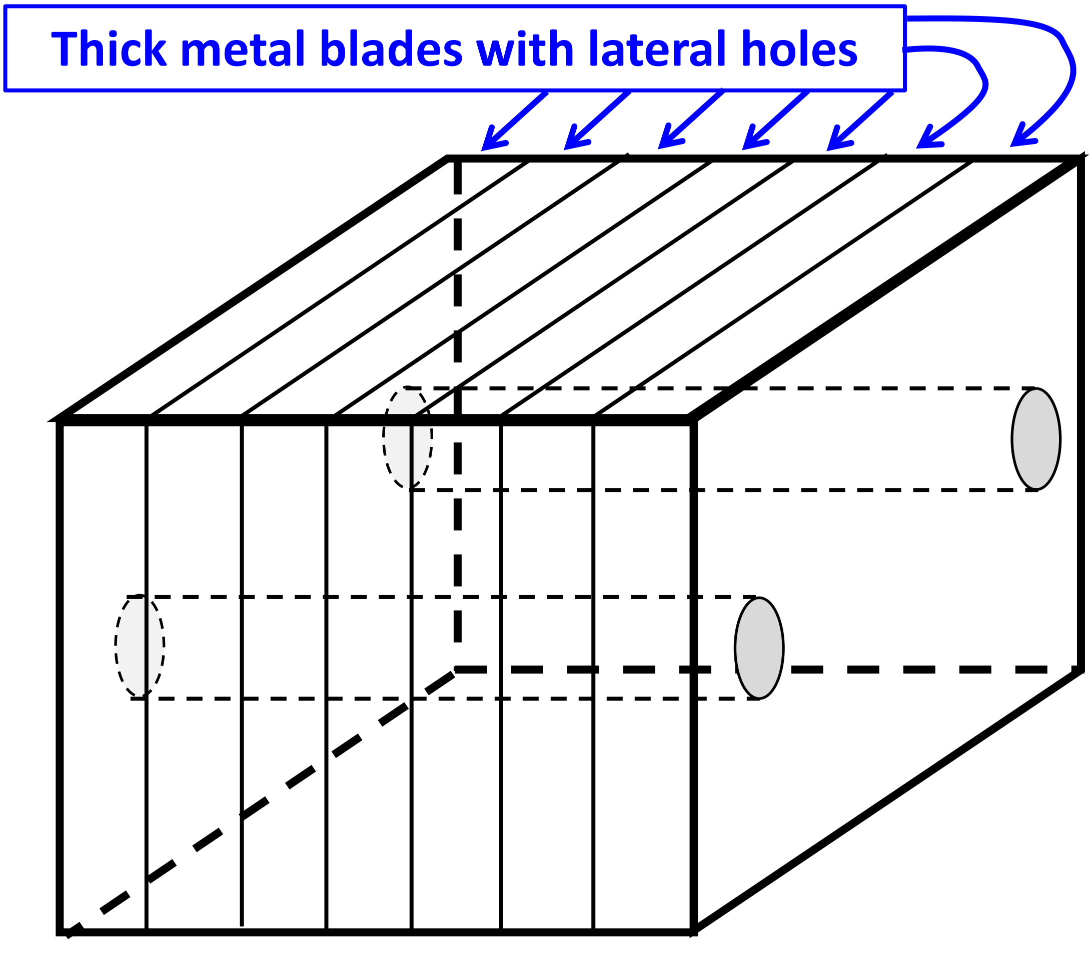

A pack of metal blades (about 2mm thick), coated with a liquid or a gel prior to mechanical squeezing by fastening screws constitutes a realistic model to illustrate the acoustic birefringence and dichroïsme of shear waves with ultrasounds in the lab.

Analog in house fractured rock model **Fig IV-2**

WEAK squeeze of the metal blades

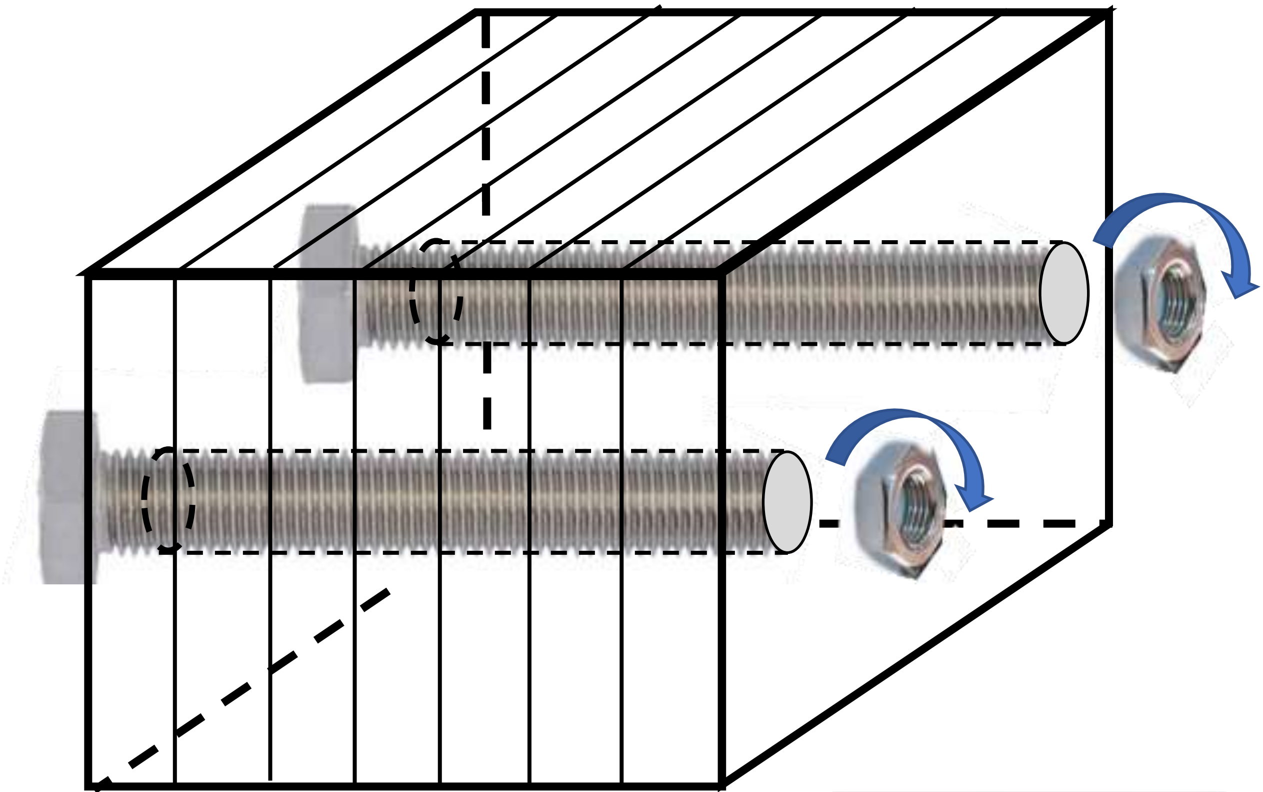

On WEAK squeeze,
The SE wave polarized to East, at right angle to the blades, is much slower than the SN wave parallel to the blades, with near NULL Amplitude.

The metal blade assemby pack is a polarizing filter for acoustc S-waves.

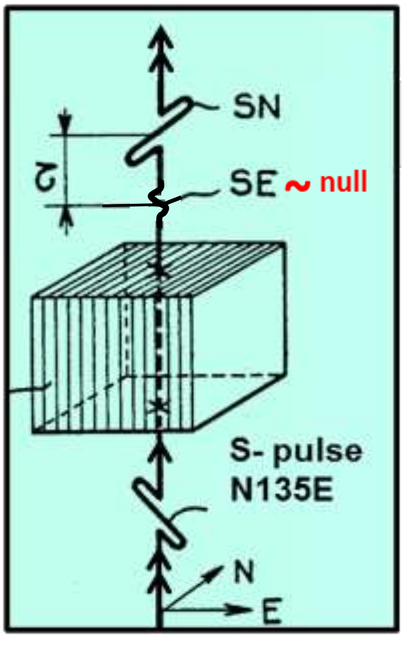

Analog in house fractured rock model Fig IV-3

MEDIUM squeeze of the metal blades,

Obtained by fastening the bolts

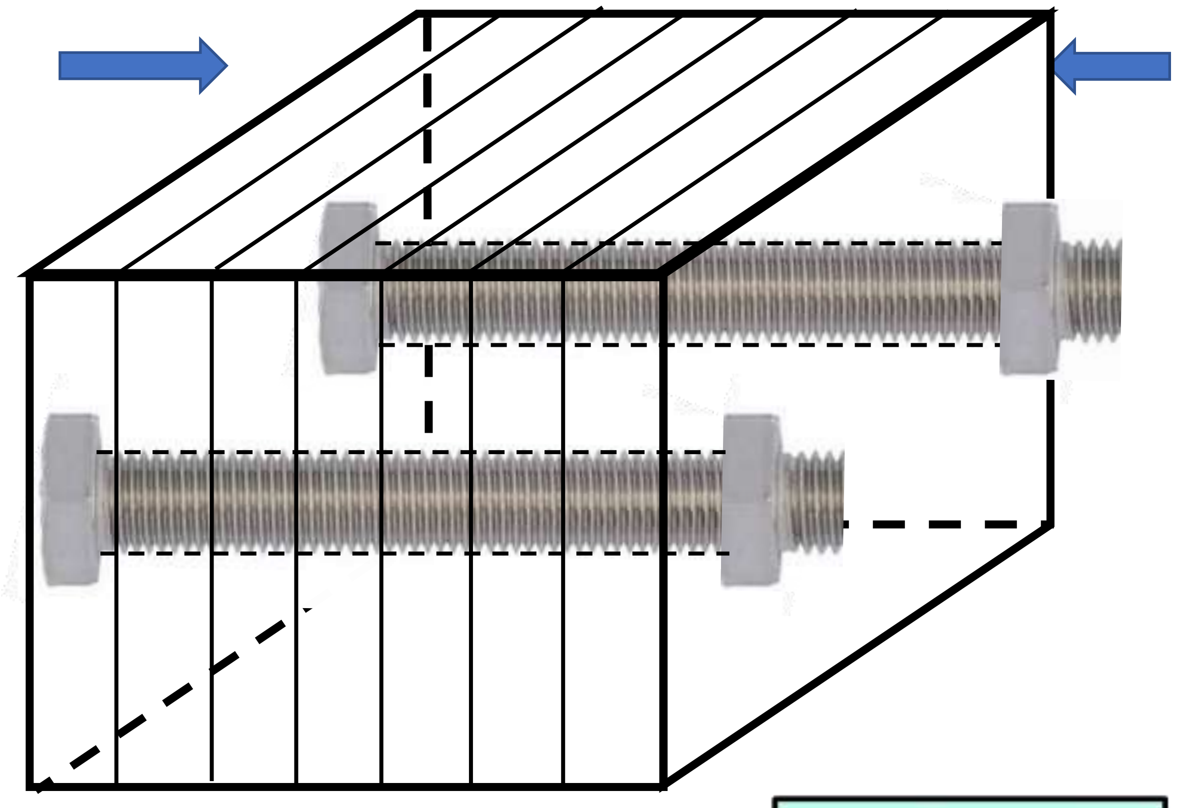

On MEDIUM squeeze,
The SE wave polarized to East,
at right angle to the blades, is
slower than the SN wave
parallel to the blades,
and with lower Amplitude

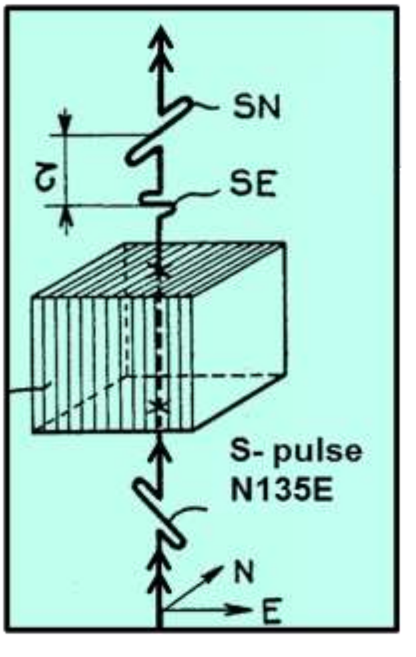

Analog in house fractured rock model **Fig IV-4**
VERY TIGHT squeeze of the metal blades,
Obtained by full fastening of the bolts

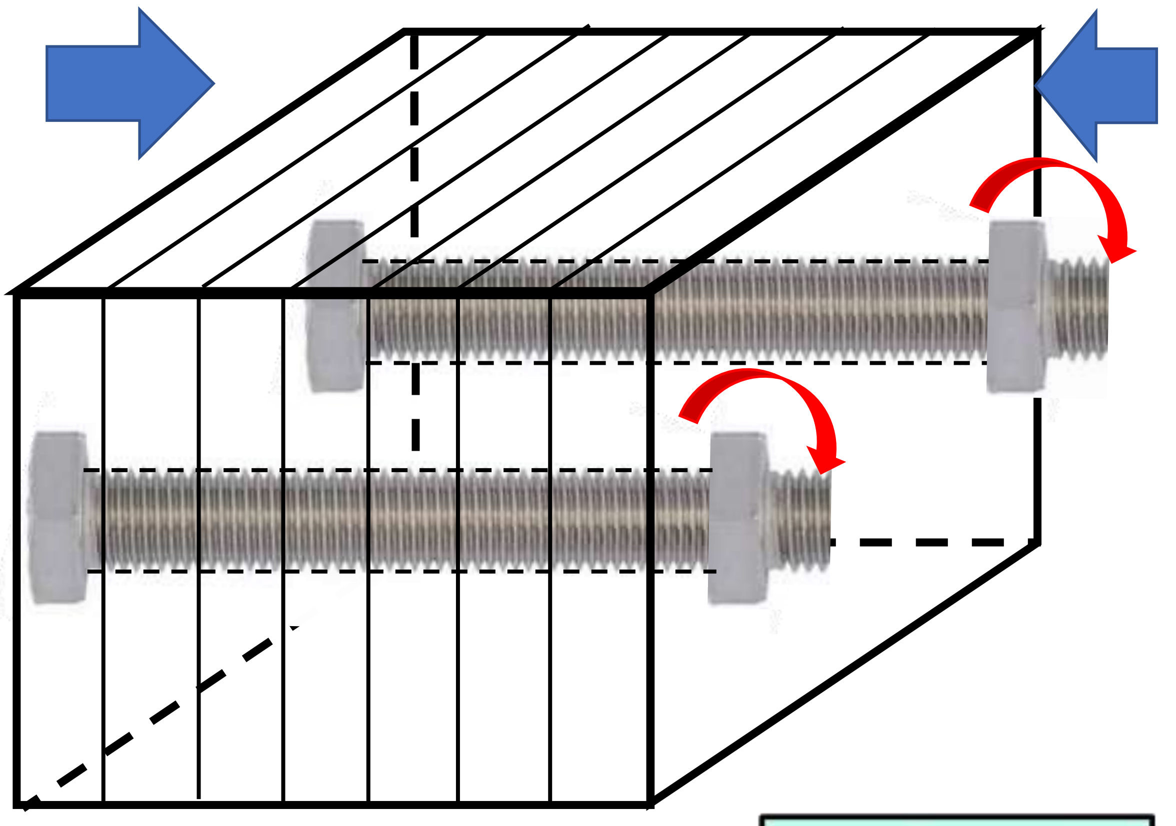

On VERY TIGHT squeeze,
The SE wave polarized to East,
is just as fast as the SN wave
parallel to the blades,
and with Same Amplitude.
The transmitted S wave has
the same polarisation as the
incident S-wave.
The medium is ISOTROPIC.

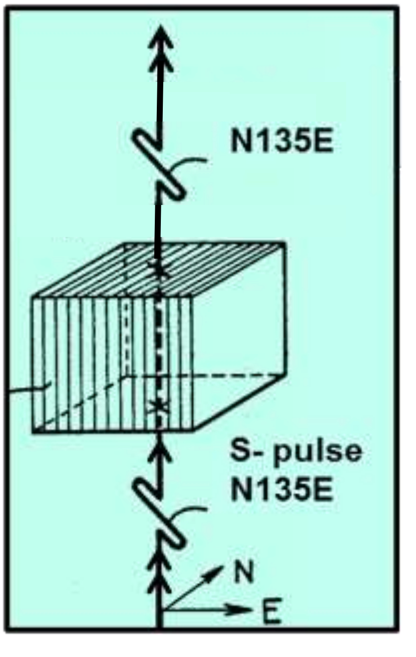

SPWLA-France workshop on Acoustics, March 31st at SGF_PARIS
Presentation by Charles Naville, IFPEN; 14h30-15h ; **S- Anisotropy**
PART-5: Case study # 3: Paris basin surface seismic, CGG-IFP

Evidence of positive and negative
Differential attenuation of split S-waves (QD)

At the end of the 1980's CGG and IFP recorded a couple of 2D surface seismic lines in the Paris Basin with strings of oriented 3 Component geophones of controlled isotropic response, using controlled field acquisition followed by specific, isotropic stack processing of the 2 oriented horizontal components .

The 2D crossline point is located on a well where S-wave anisotropy had been evidenced by a previous 3C-VSP.
Ref: Naville, C. and G. Omnès,1988. Examples of S-wave splitting analyses from VSP data, in: *Geophysical transactions,1988, Vol. 34. No. 1. pp. 121—131; https://core.ac.uk/download/pdf/195333751.pdf*

The processing results show an anisotropic corridor, 400m wide, in which the fast S-wave is oriented consistently to the NE , but becomes more attenuated than the slow S-wave from East to West inside this corridor.

Geomechanical and geological interpretations are still lacking…

Other Ref: (ultrasonic domain):
Shear-wave velocity and Q anisotropy in rocks: A laboratory study, by G. Tao and M.S. King, in International Journal of Rock Mechanics and Mining Sciences & Geomechanics Abstracts, Volume 27, Issue 5, October 1990, Pages 353-361. https://doi.org/10.1016/0148-9062(90)92710-V

Paris Basin 3C surface seismic 3C test with vertical vibrator source. **Fig V-1**

Velocity ANISOTROPY from P-S converted reflection between Surface to Kimmeridgien (~ 1000m deep)

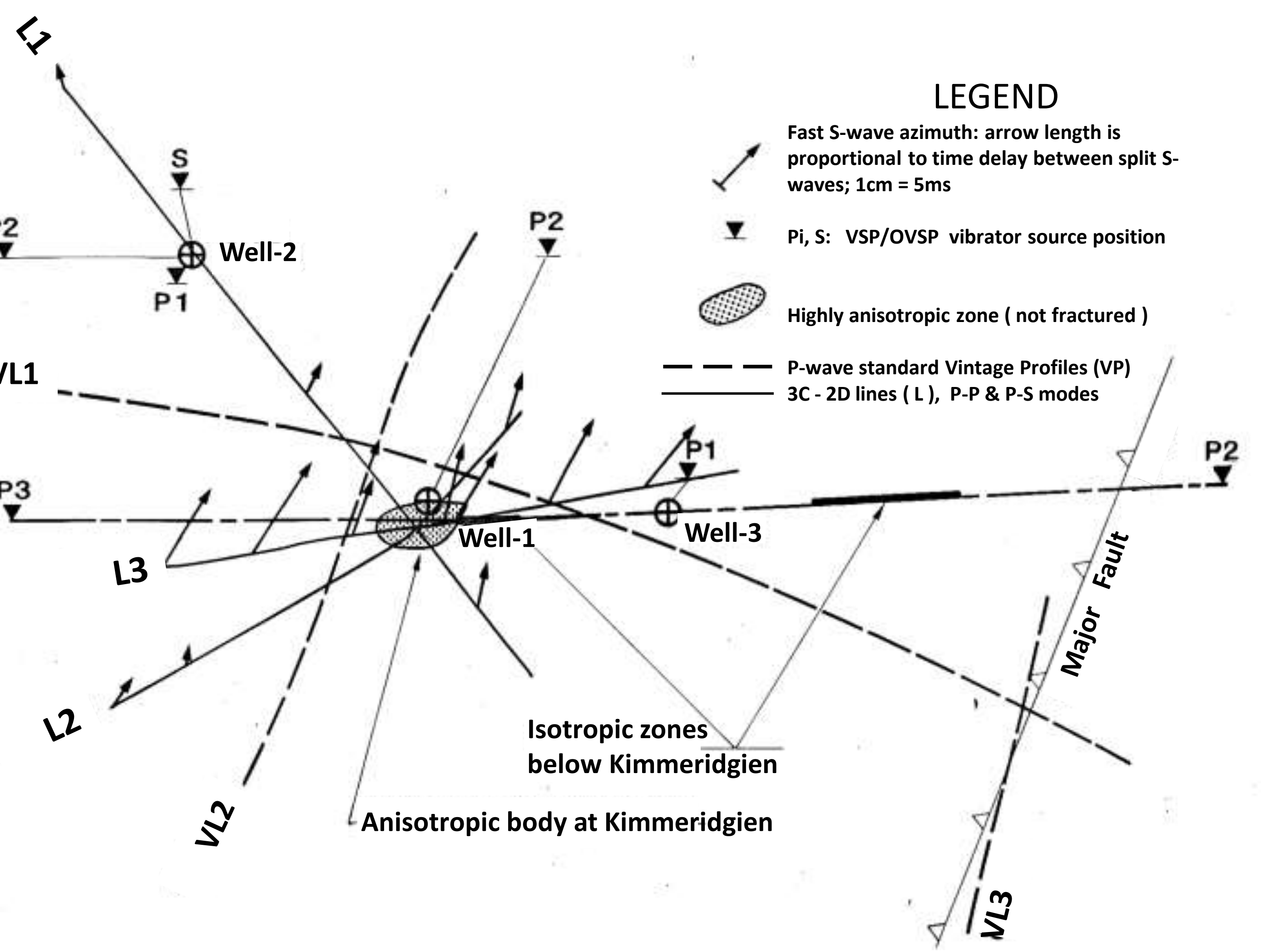

Courtesy of CGG & IFP

Paris Basin 3C surface seismic 3C test with vertical vibrator source. **Fig V-2**

Attenuation ANISOTROPY from P-S converted reflection between Surface to Kimmeridgien (~ 1000m deep)

LEGEND

QD > 0 : where the arrow is oriented in the same direction as S-fast (previous figure)

QD < 0 : where the arrow is opposite to S-fast arrow (previous figure)

QD scale: arrow length = 2 DB

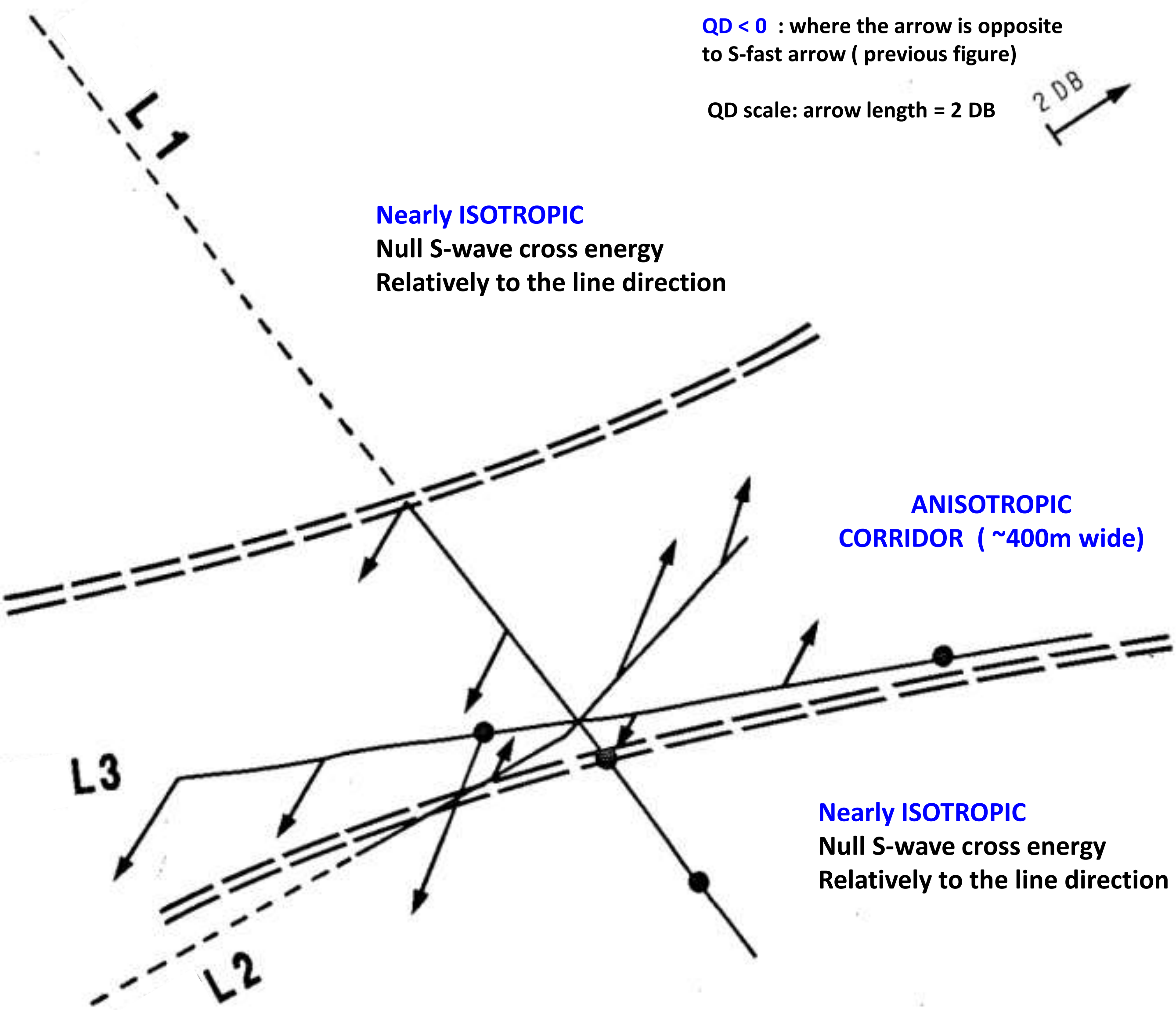

Courtesy of CGG & IFP

Paris Basin 3C surface seismic 3C test with vertical vibrator source. **Fig V-3**

Velocity and Attenuation ANISOTROPY results superimposed, between Surface to Kimmeridgien

Anisotropic Corridor in Blue limits

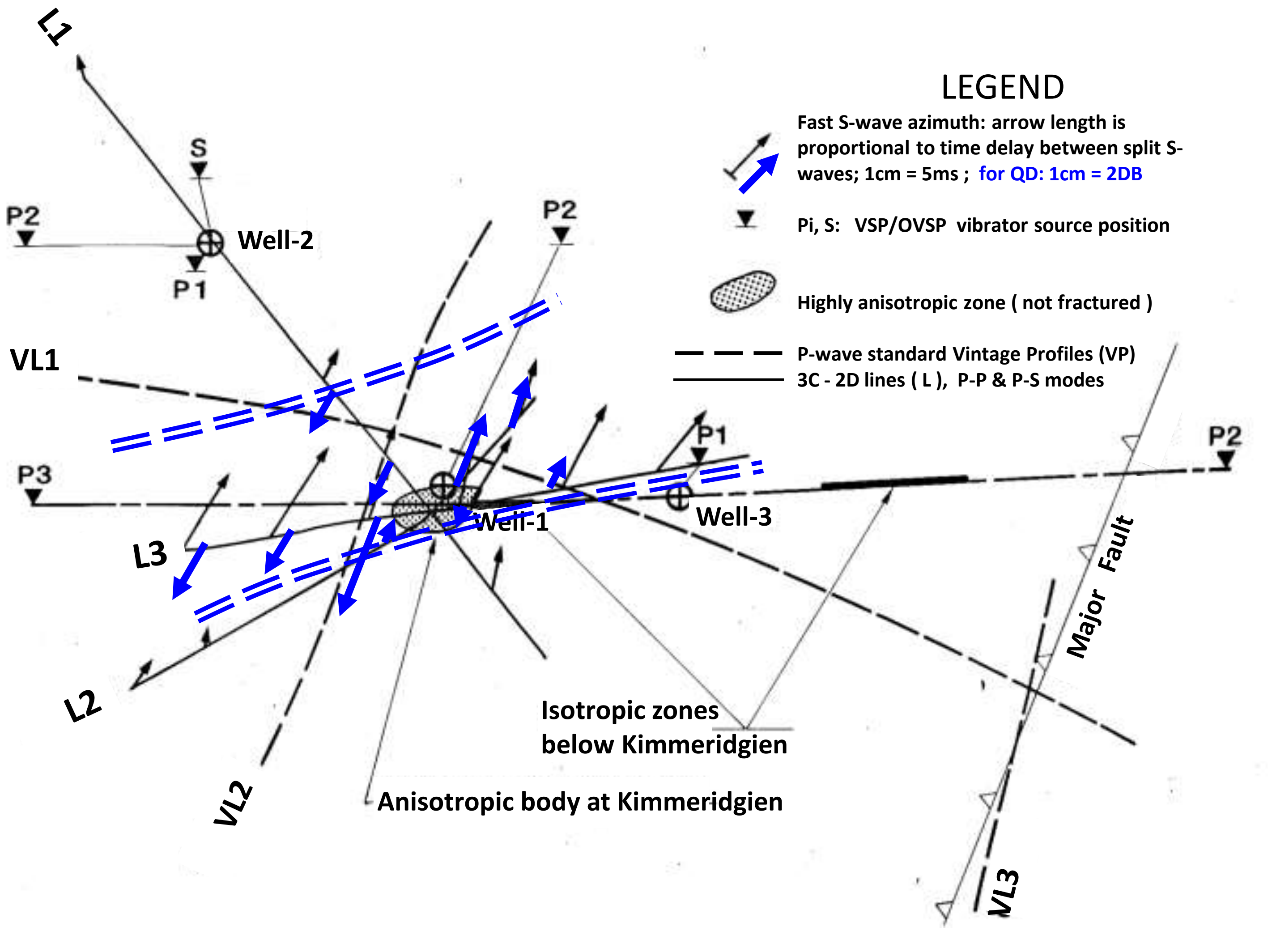

Courtesy of CGG & IFP

STRESS RELATED TO GEOLOGIC STRUCTURES Fig V-4

Basic Principles in Tectonics

by Carlos Cramez & Jean Letouzey

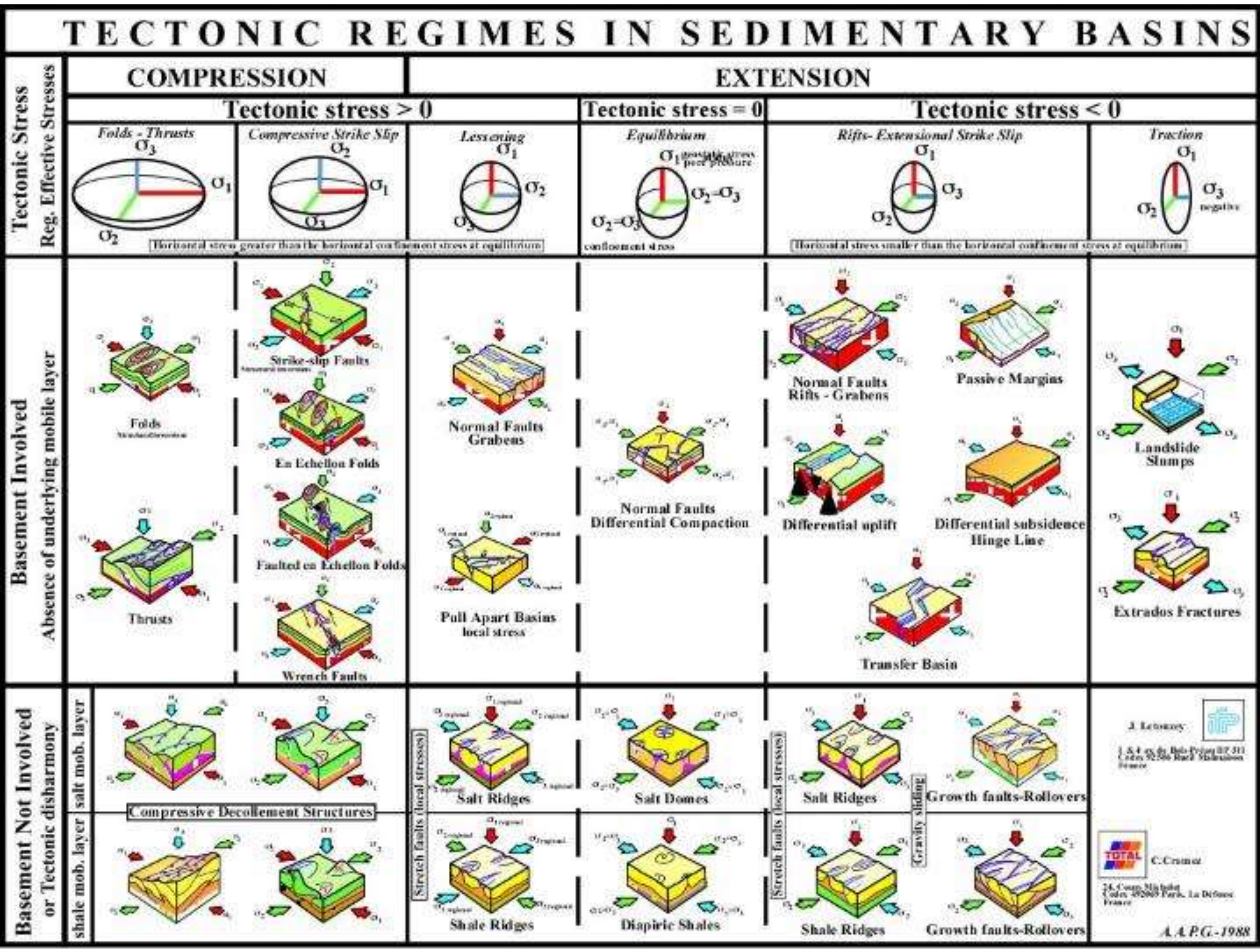

http://homepage.ufp.pt/biblioteca/WebBasPrinTectonics/BasPrincTectonics/Page1.htm

Also published in WPC: Proceedings Of The 12th World ∗petroleum∗ Congress–exploration(not Handled By Ny): 002 Hardcover – Import, 28 October 1987

SPWLA-France workshop on Acoustics, March 31st at SGF_PARIS
Presentation by Charles Naville, IFPEN; 14h30-15h ; **S- Anisotropy**
PART-6: Micellaneous on Birefringence: Way forward; Discussion

- Calibration test wells are desirable , in order to make sure that different commercial dipole sonic tools
and differing processing procedures
yield similar results, continuously versus time.

- *Monitoring birefringence in* ***boreholes located in the vicinity of major faults*** *could be useful to forecast earthquakes ?*

(SAF fault, Turkey major faults, etc…)

Fig VI-1

Test borehole model in CUP: China University of Petroleum (East China) : the logging hole in the center allows for operating any acoustic logging tool ; the rat hole at the bottom accomodates the loging tool length.

Modified from Fig.1 of Zhuang et al.: EL130 J. Acoust. Soc. Am. 146 (2), August 2019 . https://doi.org/10.1121/1.5120551

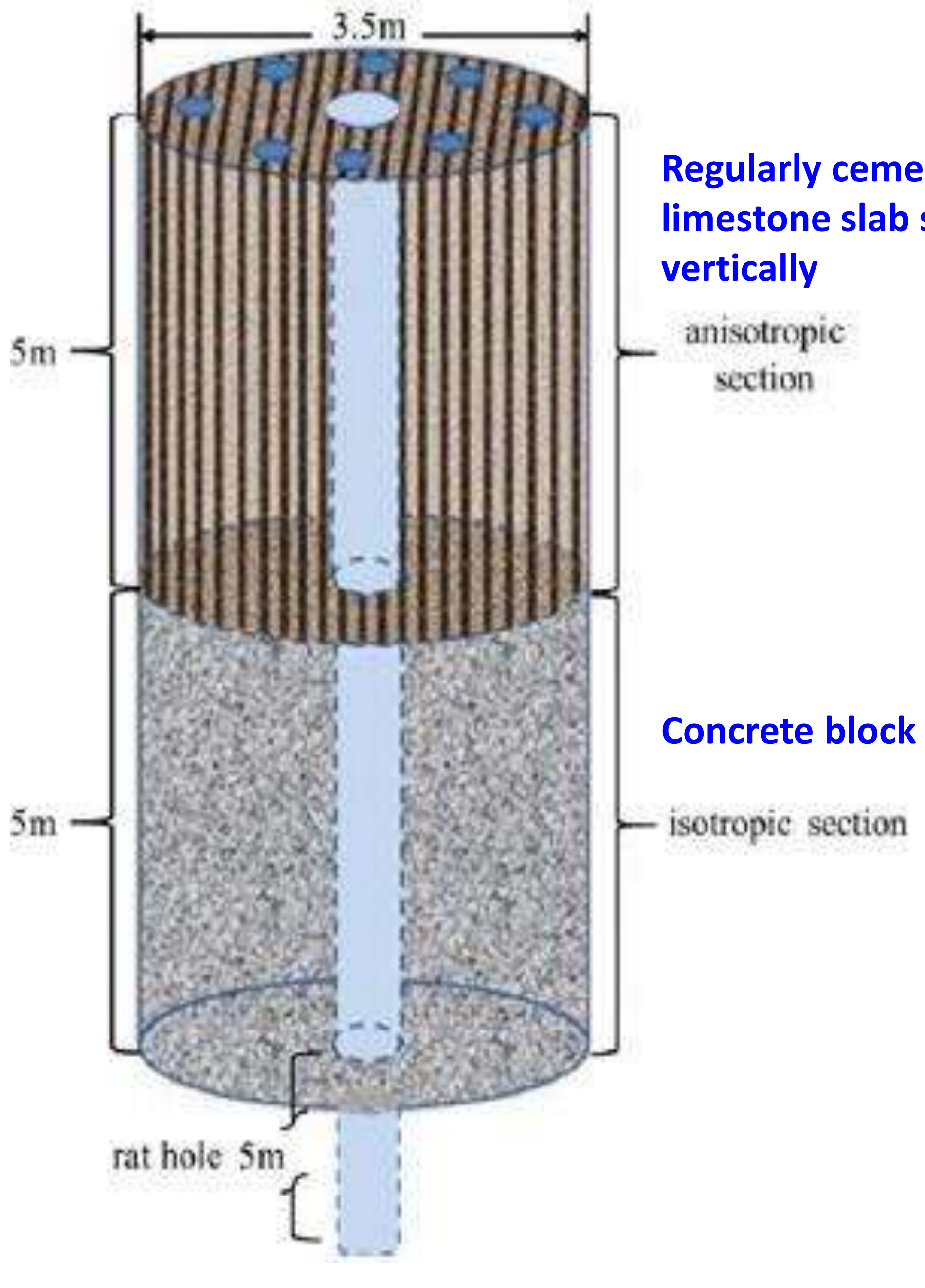

Fig VI-2

Test borehole model: the logging hole in the center allows for operating any acoustic logging tool ; the rat hole at the bottom accomodates the loging tool length.

Modified from Fig.1 of Zhuang et al.: EL130 J. Acoust. Soc. Am. 146 (2), August 2019 . https://doi.org/10.1121/1.5120551

“Azimuthal shear-wave anisotropy measurement in a borehole: Physical modeling and dipole acoustic verification »

Small peripheral holes H1-H6 contain two component sonic receivers , in the 20kHz range.

The Source and acoustic logging tools can be lowered into the central hole.

Fig VI-3

Natural site suggested for an S-wave birefringence test well aimed at the calibration of commercial dipole sonic tools and anisotropy detection processing , and for oriented 3 component VSP and S-wave birefringence detection by VSP…

The Zumaia “flytsch” shoreline site , Near Bilbao, Northern Spain, in the Basque country

Zumaia “flytsch”:
https://www.google.fr/maps/uv?pb=!1s0xd51cf9c13aa3df9%3A0xc990af9638013241!3m1!7e115!5sRecherche%20Google!15sCgIgAQ&hl=fr&imagekey=!1e10!2sAF1QipOliSna-w7sr7VmdJa1EQsJxUOmxlL7OsbwzbNh&sa=X&ved=2ahUKEwiAybW6_4b4AhVFiRoKHXIfDh8Q9fkHKAF6BAgBEAc

THANK YOU for your Attention.

charles.naville@orange.fr